

Research Paper

Design of heat exchangers using Falcon Optimization Algorithm

Emerson Hochsteiner de Vasconcelos Segundo^{a,*}, Viviana Cocco Mariani^{a,b}, Leandro dos Santos Coelho^{b,c}

^a Department of Mechanical Engineering, Pontifical Catholic University of Paraná (PUCPR), Curitiba, PR, Brazil

^b Department of Electrical Engineering, Federal University of Paraná (UFPR), Curitiba, PR, Brazil

^c Industrial and Systems Engineering Graduate Program (PPGEPS), Pontifical Catholic University of Paraná (PUCPR), Curitiba, PR, Brazil



HIGHLIGHTS

- A new metaheuristic based on the hunting behavior of falcons (FOA) is proposed.
- FOA was applied efficiently in several benchmark functions for single-objective.
- Total cost decreasing 28 and 57.8% for shell-and-tube heat exchanger cases using FOA.
- EGU units reduced 15.42% for plate-fin heat exchanger case 1 using FOA.
- Effectiveness increasing 10% for plate-fin heat exchanger case 2 using FOA.

ARTICLE INFO

Keywords:

Metaheuristics
Optimization
Falcon Optimization Algorithm
Shell-and-tube heat exchanger
Plate-fin heat exchanger

ABSTRACT

This paper proposes a novel metaheuristic optimizer based on the hunt behavior of falcons called Falcon Optimization Algorithm (FOA). FOA is a robust and powerful stochastic population-based algorithm that needs the adjustment of few parameters for its three-stage movement decision. Simulation results based on well-known twelve benchmark single-objective functions demonstrate the efficiency, effectiveness and robustness of the proposed method in comparison to other algorithms. Furthermore, the results of its single-objective application in heat exchangers shell-and-tube and plate-fin types allowed better results than previous works for the objective functions total cost for shell-and-tube heat exchanger (28% and 57.8% of reduction for cases 1 and 2, respectively) and number of entropy generation units (15.42% of reduction for case 1) and effectiveness (10% of increasing for case 2) for plate-fin heat exchanger type, alongside with a thermal-hydraulic discussion. Moreover, the FOA reached some solutions better than those previously reported in the literature.

1. Introduction

Optimization is about the search for the best possible solution (or a set of solutions in multi-objective optimization), or trade-off solutions, for a given problem with or without constraints. Over the last decades several researchers have focused their attention to develop new and efficient optimization techniques for several needs [1,2]. The major challenge of the global continuous optimization remains about those problems that present many local optima. Mathematical optimization techniques were the only methods for optimizing problems before the proposal of the metaheuristic techniques, where the mathematical optimization techniques are mostly deterministic, suffering from local minima entrapment problem. Some of them, such as gradient-based

methods that require derivative information of the search space. The referred problems make this kind of approach non-efficient algorithms for solving real problems related to global optimization [3]. However, adjoint based optimization techniques can present high efficiency for solving computationally intensive problems, such as CFD-based and even single-objective optimization problems [4]. Yet, the combination of metaheuristic optimization with gradient-based methods may lead to high efficiency techniques as well [5].

Among the wide universe of algorithms, the global optimization field based on metaheuristics has been active, generating every year different kinds of stochastic algorithms. Differently of the deterministic algorithms, stochastic techniques may find distinct solutions from the same initialization population. Metaheuristic algorithms uses the

* Corresponding author.

E-mail addresses: e.hochsteiner@gmail.com, emerson.segundo@pq.cnpq.br (E.H.d. Vasconcelos Segundo), viviana.mariani@pucpr.br (V.C. Mariani), leandro.coelho@pucpr.br (L.d.S. Coelho).

Nomenclature	
a_1	numerical constant (€)
a_2	numerical constant (€/m ²)
a_3	numerical constant
A	heat exchanger surface area (m ²)
ABC	Artificial Bee Colony
AD	awareness probability
Aff	free flow area (m ²)
$Atot$	heat exchanger surface area (m ²)
B	baffles spacing (m)
BBO	Biogeography-Based Optimization
BA	Bat Algorithm
BA	Bees Algorithm
b	constant for the shape of the logarithmic spiral
C	heat capacity rate (W/K)
c_c	cognitive constant
Ce	energy cost (€/kW h)
Ci	capital investment (€)
Co	annual operating cost (€/yr)
Cod	total discounted operating cost (€)
Cp	specific heat (J/kg K)
CSA	Cuckoo Search Algorithm
C_{tot}	total annual cost (€)
D	dimension
DE	differential evolution
de	hydraulic shell diameter (m)
d_i	tube inside diameter (m)
d_o	tube outside diameter (m)
Ds	shell internal diameter (m)
Dh	hydraulic diameter (m)
DP	dive probability
f	friction coefficient
F	temperature difference correction factor
FA	Firefly Algorithm
f_c	following constant
f_i	function to evaluate
FOA	Falcon Optimization Algorithm
G	mass flux velocity (kg/m ² s)
GA	Genetic Algorithm
g_{best}	best global position
GSA	Gravitational Search Algorithm
h	convective heat transfer coefficient (W/m ² K)
H	height of the fin (m)
H_{ot}	annual operating time (h/yr)
HSA	Harmony Search Algorithm
i	annual discount rate (%)
ICA	Imperialist Competitive Algorithm
iter	iteration
$iter_{max}$	maximum number of iterations
j	Colburn factor
k	thermal conductivity (W/m K)
l	lance length of the fin (m)
L	heat exchanger length (m)/tube length (m)
lb	lower bound
m	mass flow rate (kg/s)
n	fin frequency/number of tube passes
n_1	numerical constant
N	number of fin layers
Ns	entropy generation units
NTU	number of transfer units
Nt	number of tubes
Nu	Nusselt number
ny	equipment life (yr)
NP	number of population members (candidate solutions)
OBL	Opposition-Based Learning
OF	objective fitness
P	pressure (N/m ²)
P_{AP}	random awareness probability parameter
P_{DP}	random dive probability parameter
P_p	pumping power (W)
Pr	Prandtl number
PSO	Particle Swarm Optimization
ΔP	pressure drop (N/m ²)
Q	heat duty (W)
q	number of objectives
r	random number
$Rcte$	specific gas constant (J/kg K)
Re	Reynolds number
Rf	fouling resistance (m ² K/W)
s	fin spacing (m)
SA	Simulated Annealing
s_c	social constant
St	tube pitch (m)
t	random number/fin thickness (m)
T	temperature (K)
TLBO	Teaching-Learning-Based Optimization
ΔT_{LM}	logarithmic mean temperature difference (K)
U	overall heat transfer coefficient (W/m ² K)
ub	upper bound
v	velocity
v_i	ith hypercube
v_{max}	maximum allowed speed
x	individual position/decision variable
x_{best}	best individual position
x_{chosen}	random chosen individual position
<i>Greek letters</i>	
ε	effectiveness
μ	viscosity (N/m ² s)
ρ	density (kg/m ³)
η	overall pumping efficiency
<i>Subscripts</i>	
best	best result achieved so far
c	cold stream
h	hot stream
i	inlet
iter	current iteration
iter-1	last iteration
min	minimum
max	maximum
o	outlet
s	shell side
t	tube side
w	wall

observation of nature in physical, chemical and biological forms, basing its conception in natural phenomena or in the behavior of some species [6–8]. Actually, the modern nature-inspired methods are called metaheuristics [9]. Metaheuristic algorithms have shown to be promising

alternatives for solving optimization problems, including those which presents non-linearity and multimodality. In the last decades many algorithms were proposed and presented to the scientific community, where some of them become well-known such as Differential Evolution

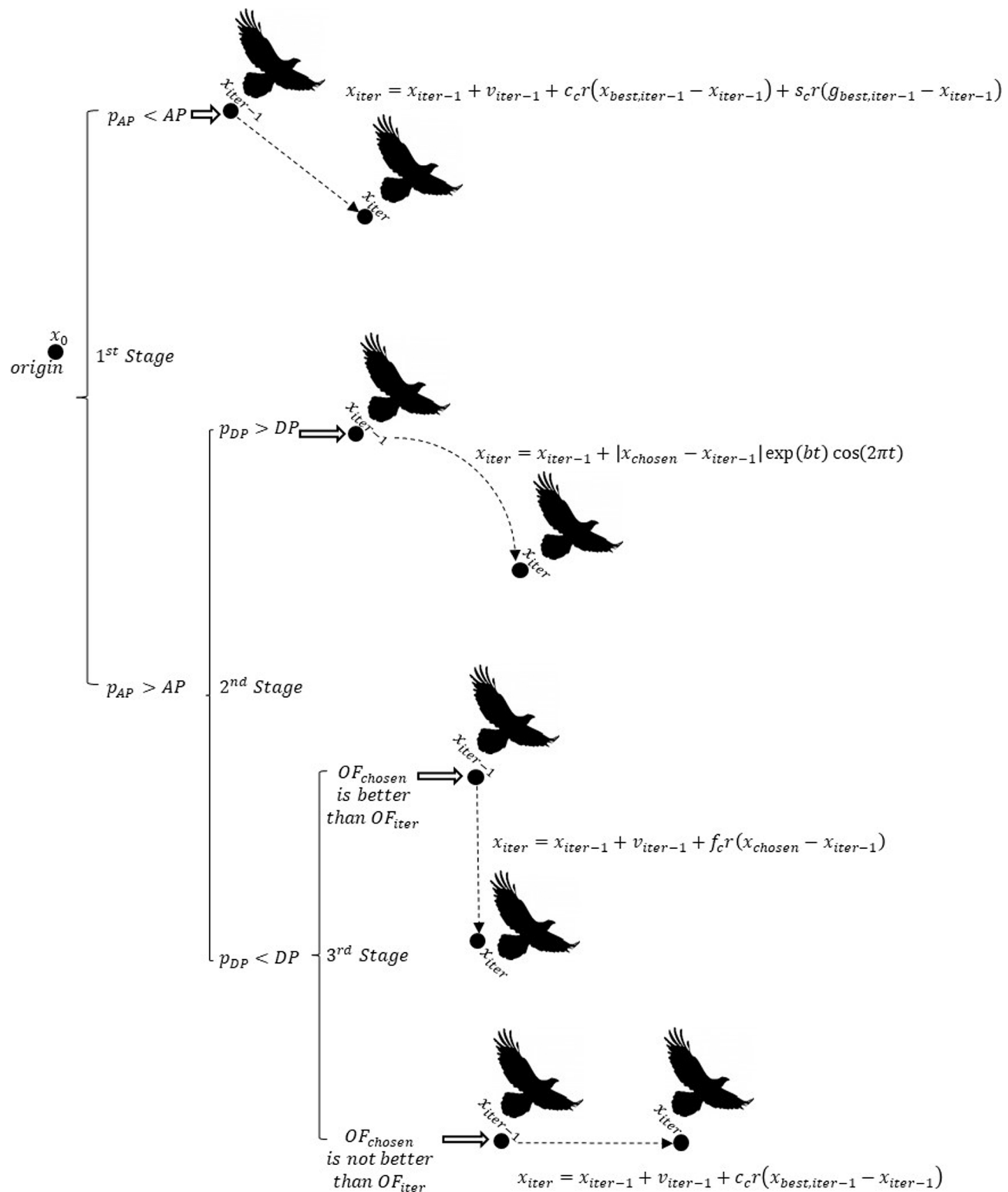


Fig. 1. Falcon hunt behavior representation where can be observed the 1st Stage (seek for preys), the 2nd Stage (adjust for dive) and 3rd Stage (proper dive condition).

(DE) [10], Genetic Algorithm (GA) [11] and Particle Swarm Optimization (PSO) [12].

This growing field enhanced the interest of many researchers around the globe to apply such techniques in engineering problems,

where heat exchangers are present. The heat exchangers most common to the investigated in the literature are the shell-and-tube and plate-fin heat types. Shell-and-tube heat exchangers is widely used in industrial processes such as condensers in nuclear power stations, steam generator

Falcon Optimization Algorithm

Step 1. Initialize parameters (control hyperparameters):
 Population size, NP ;
 Maximum number of generations, $iter_{max}$;
 Maximum allowed speed, v_{max} ;
 Values of cognitive, c_c , social, s_c , and following, f_c , constants;
 Values of awareness (AP) and dive probability (DP);
 Insert boundaries restrictions ub , upper, and lb , lower bounds, and;
 Insert objective function.

Step 2. Initialization of the population with random positions and velocities.

Step 3. In $iter = 1$ for each individual set x_{best} and its corresponding $OF_{p_{best}}$, and g_{best} and its corresponding $OF_{g_{best}}$.

Step 4. for $iter = 2$ to $iter_{max}$ do:

Step 4.1. for $i = 1$ to NP do:

- Generate random numbers p_{AP} and p_{DP} .
- Select one random individual, x_{chosen} .
- Step 4.2.** if $p_{AP} > AP$

 - Step 4.3** if $p_{DP} > DP$

 - $x_{iter} = x_{iter-1} + |x_{chosen} - x_{iter-1}| \exp(bt) \cos(2\pi t)$
 - else
 - Step 4.4.** if $OF_{chosen} < OF_{iter}$

 - $x_{iter} = x_{iter-1} + v_{iter-1} + f_c r(x_{chosen} - x_{iter-1})$
 - else
 - $x_{iter} = x_{iter-1} + v_{iter-1} + c_c r(x_{best,iter-1} - x_{iter-1})$
 - end if

 - $x_{iter} = x_{iter-1} + v_{iter-1} + c_c r(x_{best,iter-1} - x_{iter-1}) + s_c r(g_{best,iter-1} - x_{iter-1})$
 - end if

 - end if

- end for

Step 4.5. Check velocity and boundaries restrictions;

Step 4.6. Evaluate the fitness for each individual, $OF_{best,iter}$;

Step 4.7. if $OF_{best,iter} < OF_{x_{best}}$ for any particle:

- $x_{best} = x_{iter};$
- end if

Step 4.8. if any $OF_{x_{best}} < OF_{g_{best}}$:

- $g_{best} = x_{iter};$
- end if

- end for

Step 5. Output results.

Fig. 2. Pseudo code for the Falcon Optimization Algorithm.

Table 1
Single-objective benchmark test functions.

	Test function	Search space [lb, ub] ^D	Optimal value
Ackley	$f_1 = -20 \exp \left[-\frac{1}{5} \sqrt{\frac{1}{D} \sum_{i=1}^D x_i^2} \right] - \exp \left[\frac{1}{D} \sum_{i=1}^D \cos(2\pi x_i) \right] + 2 \mp e$	$[-32, 32]^{30}$	0
Alpine	$f_2 = \sum_{i=1}^D \sqrt{x_i} \sin(x_i) + 0.1x_i$	$[-10, 10]^{30}$	0
Griewank	$f_3 = \sum_{i=1}^D \frac{x_i^2}{4000} - \prod_{i=1}^D \cos\left(\frac{x_i}{\sqrt{i}}\right) + 1$	$[-600, 600]^{30}$	0
Levy	$f_4 = \sin^2(\pi w_i) + \sum_{i=1}^{D-1} (w_i - 1)^2 [1 + 10 \sin^2(\pi w_i + 1)] + (w_D - 1)^2 [1 + \sin^2(2\pi w_D)]; w_i = 1 + \frac{x_i - 1}{4}$	$[-10, 10]^{30}$	0
Powell	$f_5 = \sum_{i=1}^{D/4} [(x_{4i-3} + 10x_{4i-2})^2 + 5(x_{4i-1} - x_{4i})^2 + (x_{4i-2} - 2x_{4i-1})^4 + 10(x_{4i-3} - x_{4i})^4]$	$[-4, 5]^{30}$	0
Rastrigin	$f_6 = 10D + \sum_{i=1}^D [x_i^2 - 10 \cos(2\pi x_i)]$	$[-5.12, 5.12]^{30}$	0
Rosenbrock	$f_7 = \sum_{i=1}^{D-1} [100(x_{i+1} - x_i^2)^2 + (x_i - 1)^2]$	$[-2.048, 2.048]^{30}$	0
Salomon	$f_8 = -\cos\left(2\pi \sqrt{\sum_{i=1}^D x_i^2}\right) + 0.1 \sqrt{\sum_{i=1}^D x_i^2}$	$[-100, 100]^{30}$	0
Sphere	$f_9 = \sum_{i=1}^D x_i^2$	$[-100, 100]^{30}$	0
Styblinski-Tang	$f_{10} = \frac{1}{2} \sum_{i=1}^D (x_i^4 - 16x_i^2 + 5x_i)$	$[-5, 5]^{30}$	$\sim -39D$
Sum of Different Powers	$f_{11} = \sum_{i=1}^D x_i ^{i+1}$	$[-1, 1]^{30}$	0
Sum Squares	$f_{12} = \sum_{i=1}^D i x_i^2$	$[-5.12, 5.12]^{30}$	0

in water reactor plants under pressure and to feed water heaters among other alternative energy applications in ocean, thermal and geothermal areas [13]. Plate-fin heat exchangers is also used in several industrial processes - specially in gas-to-gas applications - in cryogenics, micro-turbines, automobiles, chemical process plants, naval and aeronautical

applications [14–16].

Taking into account the works developed and presented to the scientific community in the last decades, the shell-and-tube heat exchangers optimization aim mainly the minimization of the system cost [17–32]. In reference of single-objective optimization of shell-and-tube

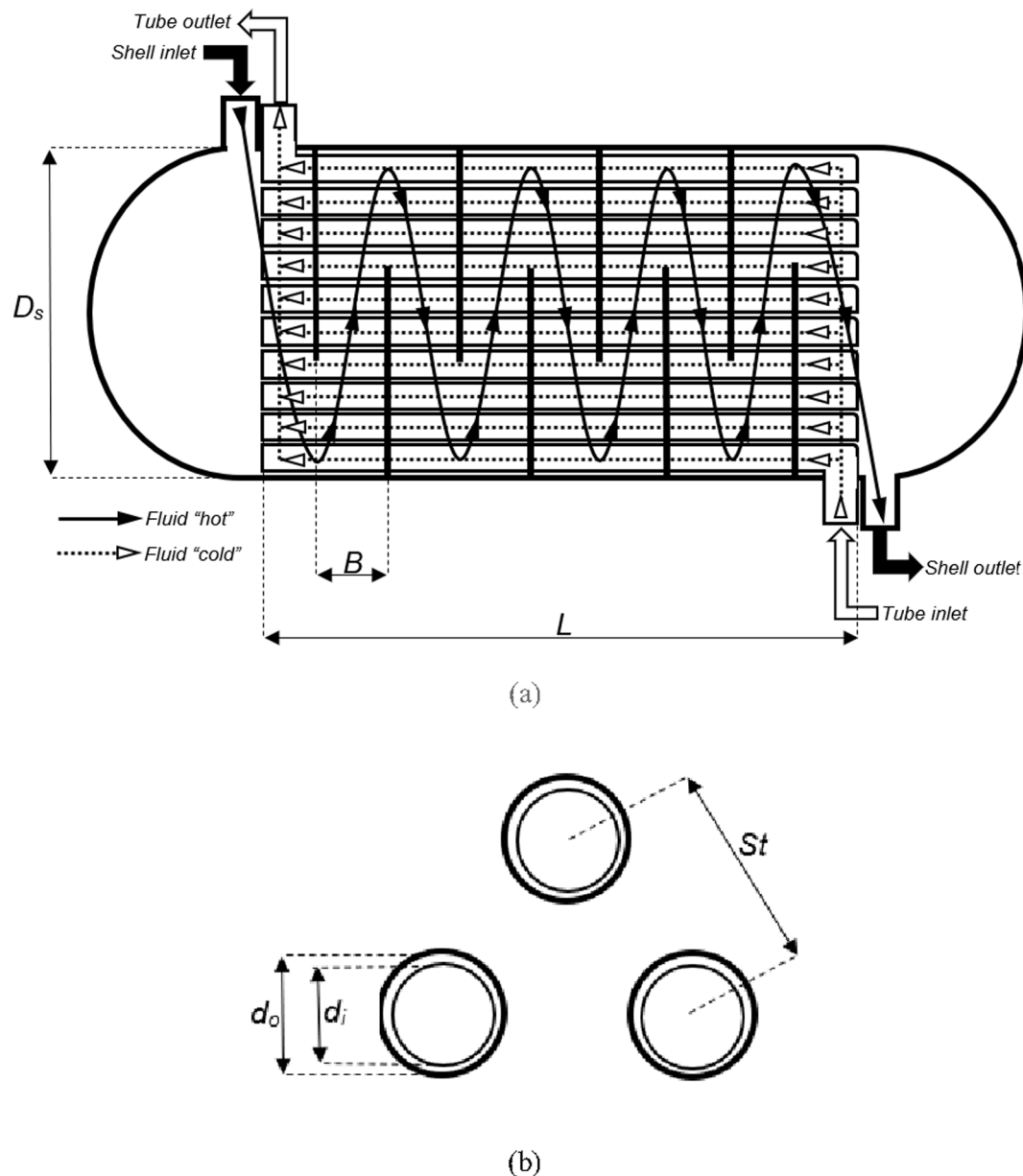


Fig. 3. (a) Typical configuration of the shell-and-tube heat exchanger. (b) Triangular tube pitch arrangement of shell-and-tube heat exchanger.

heat exchangers, several objective functions have been investigated through many metaheuristics over the last two decades. Chauduri et al. [19] investigated this type of heat exchanger using Simulated Annealing (SA), in that study was considered an optimization algorithm for large scale combinatorial problems, where the aim was the minimization of the heat transfer area e total cost. The major contribution of that work could be considered the identification of better results with the inclusion of more decision variables and configurations alternatives to the design.

Almost a decade later, Selbas et al. [20] studied the minimization of total cost utilizing GA adopting several variables such as outside diameter of the tubes, flow arrangement of the tubes, number of tube passages, outside shell diameter and baffles spacing, reaching better results than previous studies for the same cases. Caputo et al. [21], also using GA and same objective function, evaluated three different cases where inside shell diameter, outside tube diameter and baffles spacing

were adopted as design variables, achieving significant reductions in the value of total cost.

Fesanghary et al. [22], on their turn, proposed the investigation of shell-and-tube heat exchangers by Harmony Search Algorithm (HSA) minimizing total cost. In that work, a sensitivity analysis was performed to identify those geometrical parameters that less influence in the final result, reducing the amount of decision variables for the optimization. Then, Patel & Rao [23] and Sahin et al. [24] applied Particle Swarm Optimization (PSO) and Artificial Bee Colony (ABC), respectively, for cost optimization of shell-and-tube heat exchanger in the same case that Caputo et al. [21], obtaining enhancements in the results of the simulations.

A few years later, Hadidi & Nazari [25], Hadidi et al. [26] and Asadi et al. [13] studied some of the cases presented earlier in references [21] and [23] using Biogeography-Based Optimization (BBO), Imperialist Competitive Algorithm (ICA) and Cuckoo Search Algorithm (CSA),

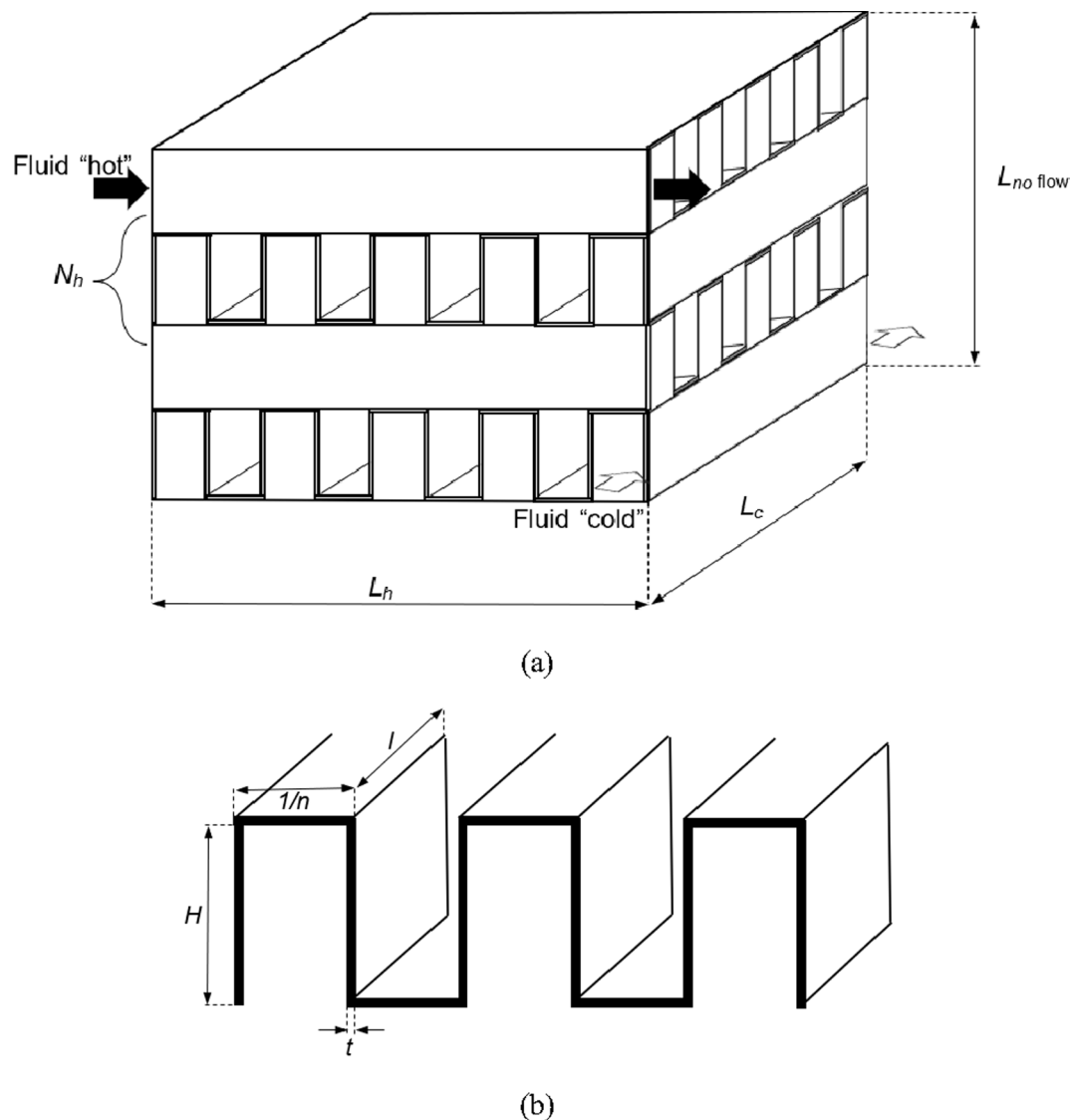


Fig. 4. (a) Arrangement of the plate-fin heat exchanger; (b) Geometrical parameters of plate-fin heat exchanger.

respectively, obtaining better results than the ones achieved by GA and PSO previously. Amini & Bazargan [27] applied a technique already used, GA, for cost and heat transfer rate, demonstrating the contradictory effect that some parameters have over both objective functions aimed. Lately, Mohanty [28,29], utilizing Firefly Algorithm (FA) and Gravitational Search Algorithm (GSA), and Vasconcelos Segundo et al. [30], using a variant of Differential Evolution, investigated shell-and-tube heat exchangers obtaining 29%, 22.4% and 26.99% of reduction, respectively, in the values of total cost in comparison to the original design. Recently, Barros et al. [31] presented a sustainability optimization of shell-and-tube heat exchanger based on Integrated Value Model for Sustainability Assessment, Petinrin et al. [32] adopted the minimization of entropy generation for shell-and-tube heat exchanger in crude oil preheat train using Firefly Algorithm.

About plate-fin heat exchangers and its optimization with meta-heuristics techniques we can cite the work of Mishra et al. [16] with GA and focusing the minimization of entropy generation units. In that study the decision variables were several geometrical parameters and a direct relation between a reduction in the entropy generation units and

the pressure drops was obtained. For the same cases, Rao & Patel [14,33] applied PSO and Teaching-Learning-Based Optimization (TLBO) and enhanced the results obtained previously with GA. Yousefi et al. [34–36], similar to previous authors, utilized ICA, GA, PSO and HSA, respectively, obtaining progressive enhancements in the results for cases studies explored previously. Recently, Zarea et al. [37] and Banoooni et al. [38] investigated plate-fin heat exchangers with the use of Bees Algorithm (BA), focusing maximization of efficiency, minimization of entropy generation units and total cost, while Vasconcelos Segundo [39] performed similar evaluation for entropy generation units through an Adaptive Differential Evolution version called JADE. Other studies such as Peng et al. [40] approached PSO for minimization of total cost, Zhang et al. [41] adopted the optimization of minimum entropy generation by a distributed parameter model, and Ghosh et al. [42] proposed a GA approach applied to maximum heat load.

The main motivation of this study is to propose a novel nature-inspired algorithm to compete with the current optimization algorithms with few adjustment parameters that can be posteriorly tuned and to be useful as basis for other algorithms that may emerge from the

Table 2

Results obtained for FOA in comparison to GA, PSO, BA and FA for the benchmark functions for best, average (avg) and standard deviation (std) values for fitness, average time processing and *p*-value Wilcoxon ranksum test.

	Criteria	f_1	f_2	f_3	f_4	f_5	f_6
GA	Best	1.3852	1.5110	0.9968	0.0168	0.1750	20.5875
	Avg.	1.8924	2.9225	1.0459	0.0497	0.4002	36.6592
	Std.	0.3452	0.8502	0.0162	0.0307	0.1625	9.9996
	Avg. time(s)	2.5885	0.5818	0.6250	1.0927	0.6339	0.5911
	<i>p</i> -value	3.7215e−07	1.3352e−09	1.2118e−12	1.2118e−12	1.2118e−12	1.5064e−05
PSO	Best	0.8612	0.8215	1.0533	0.0545	0.1899	21.0174
	Avg.	1.6623	1.8706	1.0983	2.0823	0.4050	41.1642
	Std.	0.4534	0.4575	0.0380	1.4746	0.1501	13.6616
	Avg. time (s)	7.9276	5.8609	5.8734	6.3901	5.7896	5.8557
	<i>p</i> -value	3.7215e−07	1.1863e−06	1.2118e−12	1.2118e−12	1.2118e−12	2.8291e−06
BA	Best	12.3141	23.4478	100.6721	7.2178	0.0275	49.7505
	Avg.	16.1136	30.4655	184.0465	17.9712	32.8453	91.4395
	Std.	1.3517	2.9119	46.6673	6.0254	44.9121	30.7990
	Avg. time (s)	2.5604	0.5818	0.6130	1.1401	0.5328	0.4740
	<i>p</i> -value	3.7215e−07	8.8290e−04	1.2118e−12	1.2118e−12	1.2118e−12	8.1611e−06
FA	Best	0.0093	0.5398	0.0017	0.0000	0.1473	21.8912
	Avg.	0.0134	0.9503	0.0039	0.0061	1.7444	38.4072
	Std.	0.0020	0.2912	0.0011	0.0227	1.7165	14.5257
	Avg. time (s)	4.7297	2.8078	2.8344	3.2958	2.8036	2.7552
	<i>p</i> -value	3.7215e−07	2.2623e−11	1.2118e−12	1.2118e−12	1.2118e−12	3.5656e−11
FOA	Best	0.0000	0.0000	0.0000	0.0000	0.0000	0.0000
	Avg.	2.6619	0.6183	0.0000	0.0000	0.0000	18.8216
	Std.	6.9024	0.9076	0.0000	0.0000	0.0000	14.8799
	Avg. time (s)	8.7828	7.0042	6.7995	7.3380	6.8266	6.8370
	f_7	f_8	f_9	f_{10}	f_{11}	f_{12}	
GA	Best	25.3860	16.9261	2.4142	−1174.7962	0.0000	0.0862
	Avg.	27.9151	22.5981	4.7844	−1174.4607	0.0000	0.1557
	Std.	0.8640	3.2763	1.9540	0.2332	0.0000	0.0453
	Avg. time (s)	0.5969	0.6281	0.6005	0.7833	0.6833	0.5385
	<i>p</i> -value	2.8646e−11	1.2118e−12	1.2118e−12	1.0712e−10	1.2118e−12	1.2118e−12
PSO	Best	26.3517	23.2967	3.4187	−1089.8305	0.0000	0.1493
	Avg.	28.5154	28.9801	11.9498	−1006.2565	0.0000	0.3710
	Std.	0.7806	4.1177	5.3295	41.4020	0.0000	0.1261
	Avg. time (s)	5.7698	5.9719	5.7375	5.9052	6.1714	5.7349
	<i>p</i> -value	2.8646e−11	1.2118e−12	1.2118e−12	2.9543e−11	1.2118e−12	1.2118e−12
BA	Best	23.0936	39.2966	9120.2529	−999.6799	0.0000	0.0787
	Avg.	28.3941	66.9899	18756.4165	−924.5327	0.0000	58.7502
	Std.	9.7760	12.8177	5891.0471	47.5878	0.0000	66.2120
	Avg. time (s)	0.4771	0.6224	0.4479	0.6052	0.6677	0.4531
	<i>p</i> -value	2.8646e−06	1.2118e−12	1.2118e−12	2.9543e−11	1.2118e−12	1.2118e−12
FA	Best	25.8389	4.8910	0.0013	−1132.5747	0.0000	0.0036
	Avg.	28.1003	8.6860	0.0025	−1081.2113	0.0000	0.1133
	Std.	0.9219	2.1352	0.0006	32.4674	0.0000	0.1289
	Avg. time (s)	2.7609	2.8563	2.7313	2.8755	2.9073	2.7250
	<i>p</i> -value	2.8646e−11	1.2118e−12	1.2118e−12	2.9542e−11	1.2118e−12	1.2118e−12
FOA	Best	0.0007	0.0000	0.0000	−1174.4743	0.0000	0.0000
	Avg.	1.0435	0.0000	0.0000	−1170.6883	0.0000	0.0000
	Std.	0.6704	0.0000	0.0000	1.1506	0.0000	0.0000
	Avg. time (s)	6.7094	6.9047	6.7172	6.8750	6.8948	6.6750

Best results are presented in bold font.

observation of birds of prey. The main inspiration of the proposed algorithm is the hunt behavior of the falcons.

The remainder of this paper is organized of the following form. **Section 2** presents the hunt behavior of falcons and an algorithm implementation procedure. **Section 3** presents the experimental setup and performance analysis tools. The results of the proposed algorithm for several single-objective benchmark functions and engineering problems of heat exchangers and their analysis are then provided in **Section 4** and **Section 5** concludes the work and suggests directions for future studies.

2. Falcon Optimization Algorithm

The main inspiration for the proposed algorithm and details about its implementation are presented in this section.

2.1. Hunt behavior of falcons

The inspiration of this algorithm was the hunt behavior of falcons when they are pursuing a prey in flight. Falcons are solitary and their

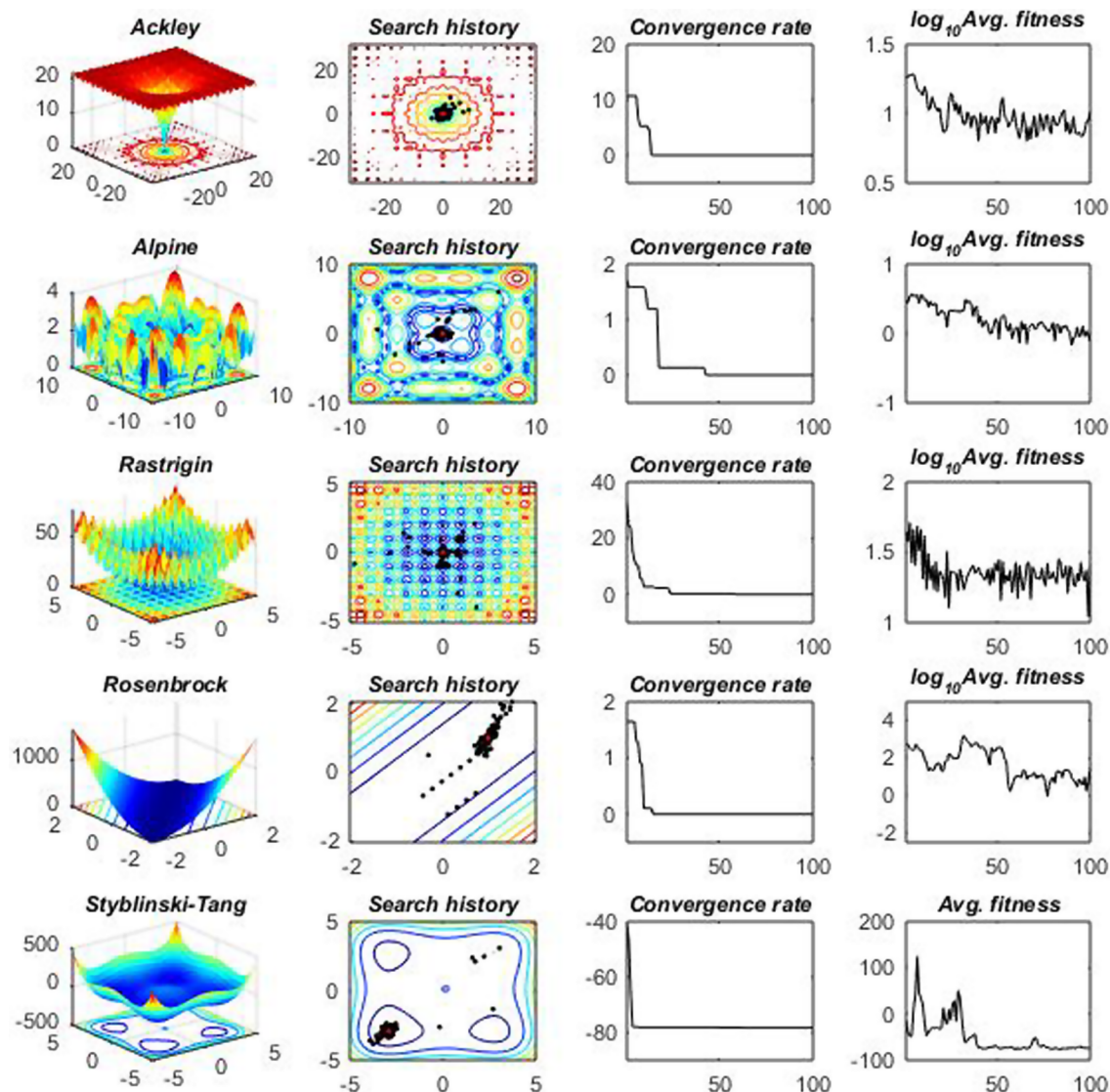


Fig. 5. Function example, search history for best candidate solution per generation (red points are the best value obtained in final generation), convergence rate and average (avg) fitness value for every multimodal function.

Table 3
Shell-and-tube inputs and physical properties of the fluids for two case studies.

Parameter	Case 1		Case 2	
	Shell side	Tube side	Shell side	Tube side
\dot{m} (kg/s)	27.80	68.90	22.07	35.31
T _i (°C)	95	25	33.9	23.9
T _o (°C)	40	40	29.4	26.7
ρ (kg/m ³)	750	995	995	995
C _p (kJ/kg K)	2.84	4.20	4.18	4.18
μ (Pa s)	0.00034	0.0008	0.0008	0.00092
μ_w (Pa s)	0.00038	0.00052	–	–
k (W/m K)	0.19	0.59	0.62	0.62
R _f (m ² K/W)	0.00033	0.0002	0.00017	0.00017

strategy of hunt are based on its needs, however these strategies follow some patterns being the principal of them the rules of flight. According to several works of Tucker [43–46] the birds of prey, in which the falcon is included, have distinct paths, curved path, to reach their prey.

The path has two segments: firstly, a logarithmic spiral along which the falcon keeps its head straight while looking sideways at the prey with maximum visual acuity, and secondly, a straight segment along which the falcon flies straight to the prey, dives when it is close enough to view the prey with binocular vision.

So, the falcons basically perform a movement that can be divided in three moments: first (1st Stage), the seek for preys, secondly (2nd Stage), the logarithmic spiral to adjust its dive and finally the third (3rd Stage), the dive itself, which can result in good result, i.e. catch a prey, if not, where the falcon simply return its movement based on its own experiences. Important to notice that the phenomena of klepto-parasitism between falcons or birds of prey are common and has received scant attention of the scientific community so far [47].

2.2. Algorithm

The step-wise procedure for the implementation of FOA is given in this subsection, where special attention is given to step 4, which holds the movements presented in the previous steps.

Table 4

Optimal geometries and thermal properties of the shell-and-tube heat exchanger case study 1.

Parameter	Original design [49]	GA [21]	PSO [23]	ICA [26]	ABC [24]	BBO [25]	CSA [13]	FOA
D_s (m)	0.894	0.830	0.810	0.879	1.3905	0.801	0.826	0.6822
L (m)	4.830	3.379	3.115	3.107	3.963	2.040	2.332	2.269
B (m)	0.356	0.500	0.424	0.500	0.4669	0.500	0.414	0.500
d_o (m)	0.020	0.016	0.015	0.015	0.0104	0.010	0.0151	0.0101
N_t	918	1567	1658	1658	1528	3587	1754	2715
v_t (m/s)	0.75	0.69	0.67	0.699	0.36	0.77	0.65	0.995
Re_t	14,925	10,936	10,503	10,429	—	7643	10,031	10,000
P_η	5.7	5.7	5.7	5.7	—	5.7	5.7	5.7
h_t (W/m ² K)	3812	3762	3721	3864	3818	4314	6104	9961
ΔP_t (Pa)	6251	4298	4171	5122	3043	6156	4186	6093
de (m)	0.014	0.011	0.0107	0.011	—	0.007	0.0107	0.0072
v_s (m/s)	0.58	0.44	0.53	0.42	0.118	0.46	0.56	0.54
Re_s	18,381	11,075	12,678	9917	—	7254	13,716	8677
P_κ	5.1	5.1	5.1	5.1	—	5.1	5.1	5.1
h_s (W/m ² K)	1573	1740	1950.8	1740	3396	2197	2083	2381
ΔP_s (Pa)	35,789	13,267	20,551	12,367	8390	13,799	22,534	17,496
U (W/m ² K)	615	660	713.9	677	832	755	848.2	888.5
A (m ²)	278.6	262.8	243.2	256.6	—	229.95	209.1	195.5
Ci (€)	51,507	49,259	46,453	48,370	44,559	44,536	40,343.70	39,513
Cod (€)	12,973	5818	6778.2	5995	6233.8	6046	7281.40	6906
$Ctot$ (€)	64,480	55,077	53,231	54,366	50,793	50,582	47,625.10	46,419

Best result is in bold font.

Table 5

Optimal geometries and thermal properties of the shell-and-tube heat exchanger case study 2.

Parameter	Original design [55]	GA [21]	PSO [23]	ABC [24]	BBO [25]	FOA
D_s (m)	0.387	0.62	0.59	1.0024	0.55798	0.520
L (m)	4.88	1.548	1.45	2.4	1.133	1.2316
B (m)	0.305	0.44	0.423	0.354	0.5	0.500
d_o (m)	0.013	0.016	0.0145	0.0103	0.01	0.0120
N_t	160	803	894	704	1565	1017
v_t (m/s)	1.76	0.68	0.74	0.36	0.898	0.9580
Re_t	36,400	9487	9424	—	7804	10,000
P_η	6.2	6.2	6.2	—	6.2	6.2
h_t (W/m ² K)	6558	6043	5618	4438	9180	9317.3
ΔP_t (Pa)	62,812	3673	4474	2046	4176	4591
de (m)	0.013	0.011	0.0103	—	0.0071	0.0086
v_s (m/s)	0.94	0.41	0.375	0.12	0.398	0.4265
Re_s	16,200	8039	4814	—	3515	4568
P_κ	5.4	5.4	5.4	—	5.4	5.4
h_s (W/m ² K)	5735	3476	4088.3	5608	4911	4682.6
ΔP_s (Pa)	67,684	4365	4721	2716	5917	5523
U (W/m ² K)	1471	1121	1177	1187	1384	1369.5
A (m ²)	46.6	62.5	59.15	—	55.73	47.65
Ci (€)	16,549	19,163	18,614	17,893	18,059	16,723
Cod (€)	27,440	1671	1696	1584.2	1251.5	1837.3
$Ctot$ (€)	43,989	20,834	20,310	19,478	19,310	18,560.3

Best result is in bold font.

Step 1: Initialize problem data and adjustable control parameters

The optimization problem, decision variables and constraints are defined. Then, the adjustable parameters of FOA such as quantity of falcons (NP), maximum allowed speed (v_{max}), values of cognitive (c_c), social (s_c), following (f_c) constants and awareness and dive probabilities (AP , DP) are provided.

Step 2: Initialize position and velocity of the falcons

The falcons are randomly positioned (using generation of random values with uniform distribution) in a D -dimensional space respecting the boundary conditions, generating the matrix:

$$x = \begin{bmatrix} x_{1,1} & \cdots & x_{1,D} \\ \vdots & \ddots & \vdots \\ x_{NP,1} & \cdots & x_{NP,D} \end{bmatrix} \quad (1)$$

where x is the falcon position, respecting the quantity of NP candidates in all its D dimensions.

The velocities are randomly generated between the v_{max} and the v_{min} restrictions, where both are determinate respecting:

$$v_{max} = 0.1ub \quad (2)$$

$$v_{min} = -v_{max} \quad (3)$$

where v_{max} and v_{min} are the maximum and minimum velocities allowed, respectively, and ub is the upper bound limit range of the problem for each dimension.

Step 3: Evaluate fitness and find global and individual best positions

For each falcon the fitness value (of) for the problem is obtained, generating the vector:

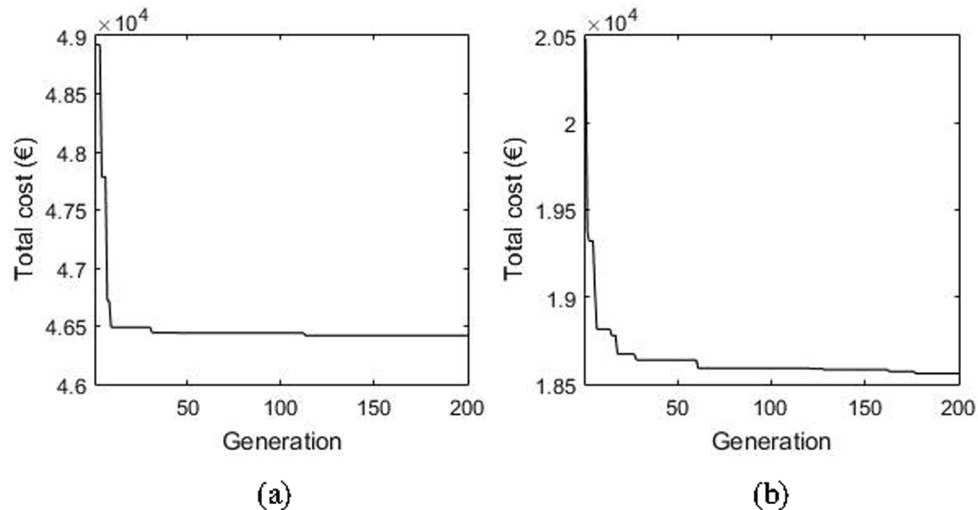


Fig. 6. Convergence rate of the best simulation obtained by FOA for the shell-and-tube heat exchanger study (a) case 1 and (b) case 2.

$$OF = \begin{bmatrix} of_1 \\ \vdots \\ of_2 \end{bmatrix} \quad (4)$$

Then, the best individual is set to be the g_{best} position and for each falcon its best individual position is set as x_{best} . These positions will be used to generate the new positions according to the logic that rules the movement behind the awareness and the dive probabilities.

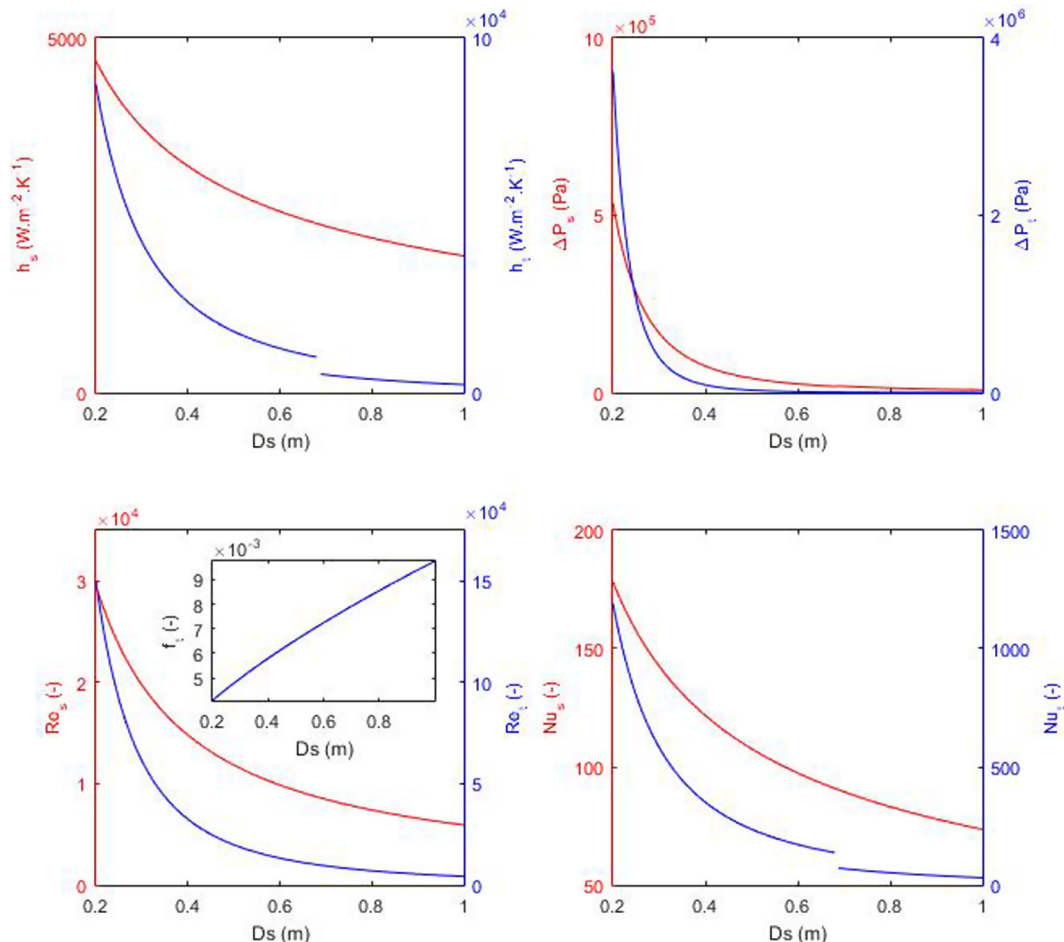


Fig. 7. Variation of the shell diameter D_s in limit range and its influence in convective heat transfer coefficients, pressure drops, Reynolds and Nusselt numbers for the shell-and-tube heat exchanger study case 1 (red lines for shell side and blue line for tube side). The discontinuity of the curves for the convective heat transfer coefficient and Nusselt number for the tube side are consistent to the flow regime changes for the shell-and-tube heat exchanger model adopted.

Step 4: Generate new positions and update the falcon positions

At first, two random numbers (p_{AP} , p_{DP}) are generated with uniform distribution for each falcon for the comparison with awareness and dive probabilities. Then the first probability compared is the awareness probability, where if p_{AP} is lower than AP the falcon performs a movement of seeking for preys according to its experience and the other falcon experiences:

$$x_{iter} = x_{iter-1} + v_{iter-1} + c_c r(x_{best,iter-1} - x_{iter-1}) + s_c r(g_{best,iter-1} - x_{iter-1}) \quad (5)$$

where x_{iter-1} and v_{iter-1} are the current position and velocity of the falcon, respectively. The procedure described is similar to the search performed by the PSO algorithm.

If p_{AP} is higher than AP , then the dive probability is compared with p_{DP} . If p_{DP} is higher than DP , then the falcon targets one chosen prey (x_{chosen}) and performs its initial movement for hunting, the logarithmic spiral given by:

$$x_{iter} = x_{iter-1} + |x_{chosen} - x_{iter-1}| \exp(bt) \cos(2\pi t) \quad (6)$$

where b is a constant defining the shape of the logarithmic spiral, equals to 1, and t is a random number in the range $[-1, 1]$ that defines how much the next position of the falcon would be close to its actual target.

If p_{AD} is lower than AP , then the fitness of the chosen prey is compared to the fitness of the falcon where if the prey is fittest it will be followed by the falcon, similar to a dive movement:

$$x_{iter} = x_{iter-1} + v_{iter-1} + f_c r(x_{chosen} - x_{iter-1}) \quad (7)$$

If not, the falcon performs a movement according to its own individual best position:

$$x_{iter} = x_{iter-1} + v_{iter-1} + c_c r(x_{best,iter-1} - x_{iter-1}) \quad (8)$$

The representation of the falcon's movement, according to the previous description, is presented in Fig. 1.

The new position obtained are then checked concerning velocities and boundary conditions. After, its new fitness values are computed and the new values of g_{best} and x_{best} are obtained. Important to notice that in all procedure described in Step 4, while analyzing one candidate solution it is considered the phenomena of klepto-parasitism between falcons. This consideration allows that at each generation one falcon may consider all others as potential targets, even preys, for the several movements performed.

Step 5: Finally, after all the evaluations the process is continued until the maximum number of iterations ($iter_{max}$) thus repeating the Step 4. The pseudo code of the Falcon Optimization Algorithm (FOA) is shown in Fig. 2.

3. Experimental setup and heat exchangers models

It has been proved that no search algorithm is the best on average for all problems of optimization [48]. An algorithm may solve some problems better and some problems worst in comparison to other

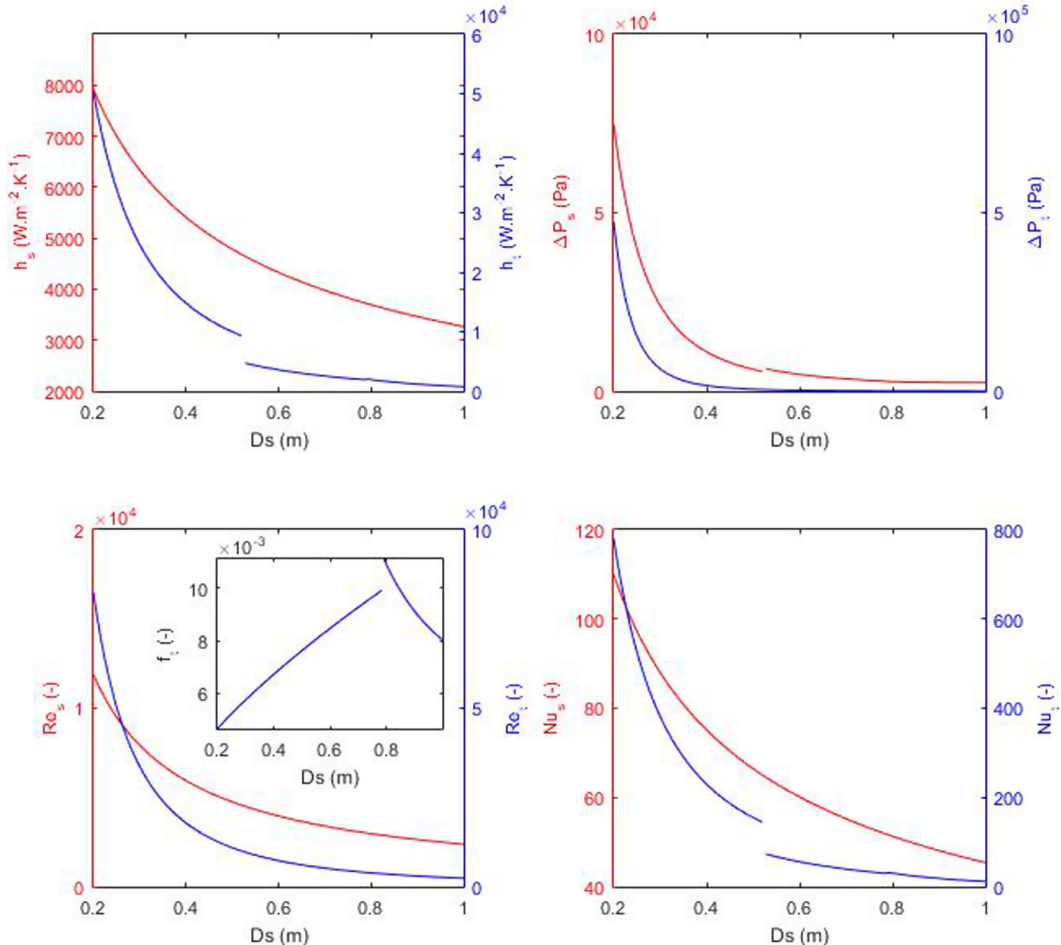


Fig. 8. Variation of the shell diameter D_s in limit range and its influence in convective heat transfer coefficients, pressure drops, Reynolds and Nusselt numbers for the shell-and-tube heat exchanger study case 2 (red line for shell side and blue line for tube side). The discontinuity of the curves for the convective heat transfer coefficient, friction coefficient and Nusselt number for tube side and pressure drop for shell side are consistent to the flow regime changes for the shell-and-tube heat exchanger model adopted.

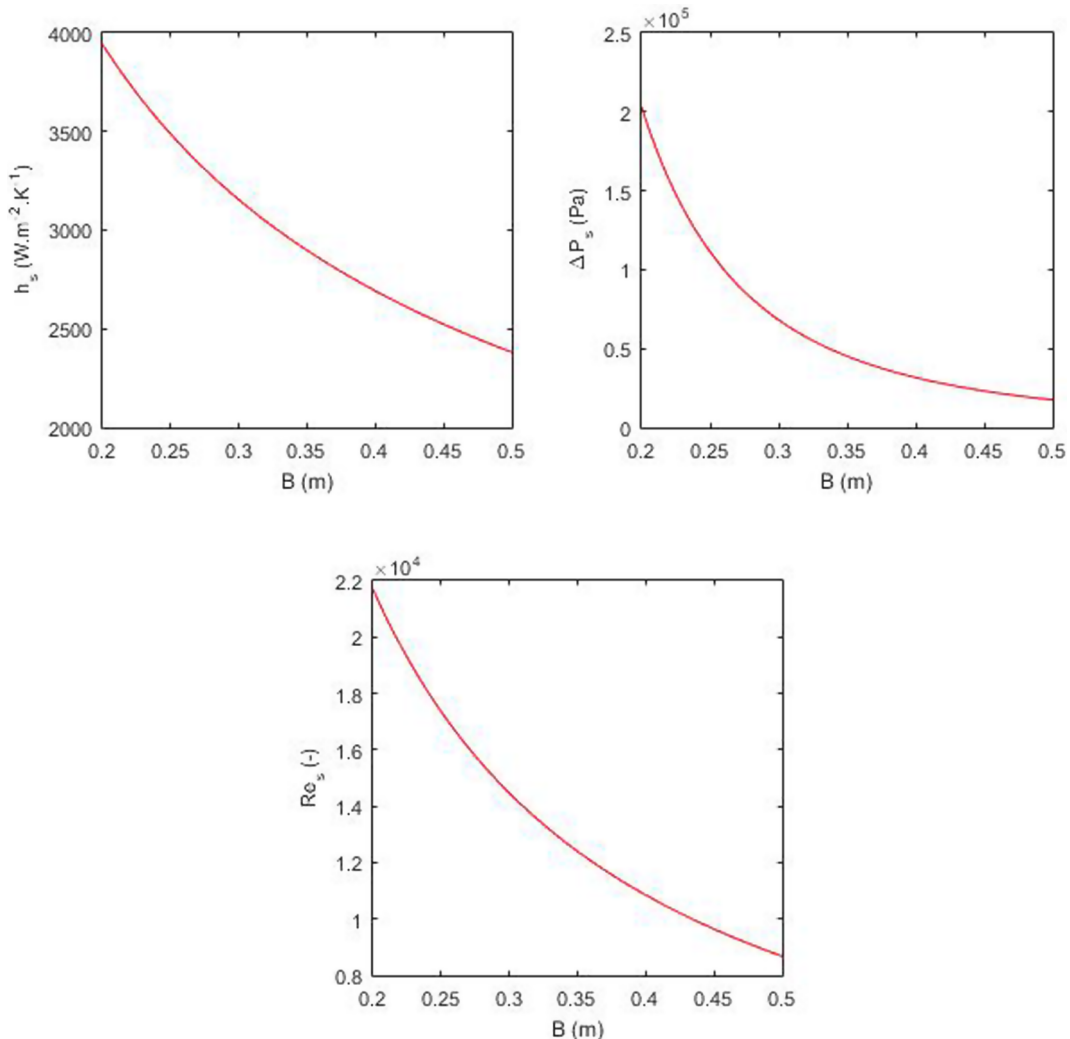


Fig. 9. Variation of the baffle spacing B in limit range and its influence in convective heat transfer coefficient, pressure drop and Reynolds number for the shell side for the shell-and-tube heat exchanger study case 1.

algorithms depending to the characteristics of the problem. The evaluations of the optimization performance of the proposed FOA were made considering a set of benchmark functions, twelve functions for single-objective optimization, and four engineering problems of heat exchangers regarding shell-and-tube and plate-fin heat types.

All the evaluated problems have different natures of objective functions, range of the decision variables and engineering problems that presents boundary constraints. Falcon Optimization Algorithm has been executed in the MATLAB® computational environment on a computer with i7-5500U 2.4 GHz processor with 16 GB RAM (Random Access Memory). For the benchmark functions simulations were performed 30 independent runs, with initial population of 30 individuals and maximum number of generations of 1000. However, for the engineering problems 50 independent runs were performed, initial population of 10D, with generations maximum number of 200. In FOA were adopted c_c , s_c and f_c equals to 2, $AP = 0.2$ and $DP = 0.8$ for all simulations and case studies investigated.

3.1. Benchmark functions

The benchmark functions are shown in Table 1 and each have different characteristics such as continuous, separable, differentiable, scalable, unimodal or multimodal. The unimodal functions are suitable for evaluating the exploitation of the optimization techniques since they have one global optimum and no local optima, while multimodal

functions are suitable for evaluating exploration and local optima avoidance as they have many local spots [3].

3.2. Heat exchangers models

The following subsection provides the mathematical models for the heat exchangers shell-and-tube and plate-fin, respectively.

3.2.1. Shell-and-tube heat exchanger

The thermal modeling of the shell-and-tube heat exchangers were taken from [30] and its design and geometrical parameters are presented in Fig. 3a and b, respectively.

Depending of the flow regime, the tube side heat transfer coefficient and friction factor are calculated by,

$$h_t = \begin{cases} \left(\frac{k_t}{d_t}\right) \left[3.657 + \frac{0.0677 \left(Re_t Pr_t \left(\frac{d_t}{L}\right)\right)^{1.33}}{1 + 0.1 Pr_t \left(Re_t \left(\frac{d_t}{L}\right)\right)^{0.3}} \right], & Re_t \leq 2100 \\ \left(\frac{k_t}{d_t}\right) \left[\frac{\frac{f_t}{2} (Re_t - 1000) Pr_t}{1 + 12.7 \sqrt{\frac{f_t}{2}} (Pr_t^{0.66} - 1)} \right], & 2100 < Re_t < 10000 \\ 0.027 \left(\frac{k_t}{d_t}\right) Re_t^{0.8} Pr_t^{0.33} \left(\frac{\mu_t}{\mu_{wt}}\right)^{0.14}, & Re_t \geq 10000 \end{cases} \quad (9)$$

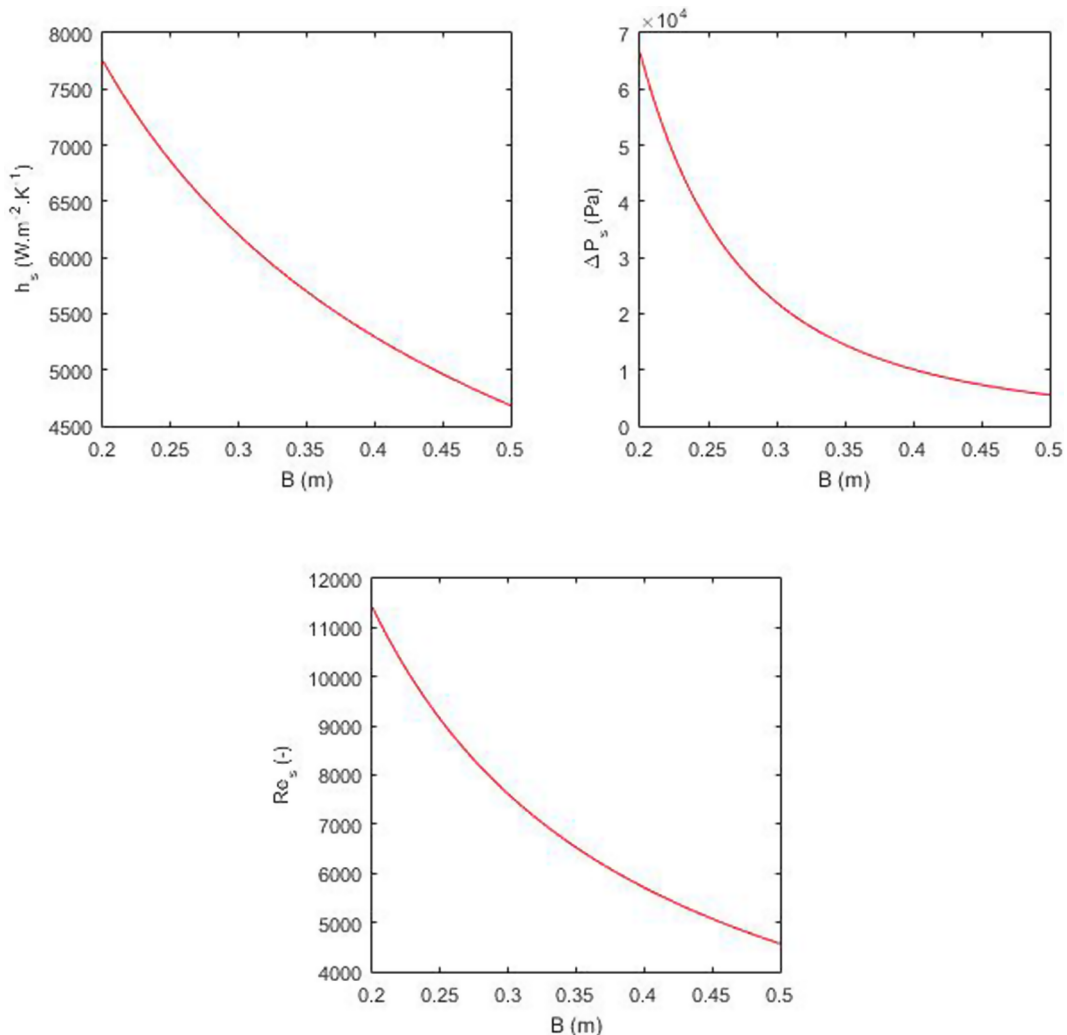


Fig. 10. Variation of the baffle spacing B in limit range and its influence in convective heat transfer coefficient, pressure drop and Reynolds number for the shell side for the shell-and-tube heat exchanger study case 2.

$$f_t = \begin{cases} (1.82\log(Re_t) - 1.64)^{-2}, & Re_t \leq 2100 \\ 0.0054 + 0.0000023(Re_t^{3/2}), & 2100 < Re_t < 4000 \\ 0.00128 + 0.1143(Re_t^{-1/3.214}), & Re_t \geq 4000 \end{cases} \quad (10)$$

where k_t and f_t are the tube thermal conductivity and friction factor, respectively.

The shell side heat transfer coefficient is given as,

$$h_s = 0.36 \left(\frac{k_s}{de} \right) Re_s^{0.55} Pr_s^{0.33} \left(\frac{\mu_s}{\mu_{ws}} \right)^{0.14} \quad (11)$$

where de is the shell hydraulic diameter, or equivalent diameter, given by [49]

$$de = \frac{1.11}{d_o} (St^2 - 0.917 d_o^2) \quad (12)$$

where $St = 1.25d_o$.

The Reynolds number for tube (Re_t) and shell (Re_s) sides can be computed by,

$$Re_t = \frac{\rho_t v_t d_i}{\mu_t} \quad (13)$$

$$Re_s = \frac{\dot{m}_s de}{A_s \mu_s} \quad (14)$$

Also, the Nusselt Number for tube (Nu_t) and shell (Nu_s) sides can be obtained by,

$$Nu_t = \frac{h_t d_i}{k_t} \quad (15)$$

$$Nu_s = \frac{h_s de}{k_s} \quad (16)$$

The flow velocities for the tube (v_t) and shell (v_s) sides are given by,

$$v_t = \frac{\dot{m}_t}{\left(\frac{\pi}{4}\right) d_i^2 \rho_t} \left(\frac{n}{Nt} \right) \quad (17)$$

$$v_s = \frac{\dot{m}_s}{\rho_s A_s} \quad (18)$$

where n is the number of tube passes, d_i is the tube inside diameter ($d_i = 0.8d_o$) and Nt is the number of tubes, determined by,

$$Nt = K_1 \left(\frac{Ds}{d_o} \right)^{n_1} \quad (19)$$

where K_1 and n_1 are coefficients determined based on the flow arrangement (shown in Fig. 3b) and number of passes, where for the studied case, the values are equals to 0.249 and 2.207, respectively, while A_s is the cross-sectional area normal to flow direction given by,

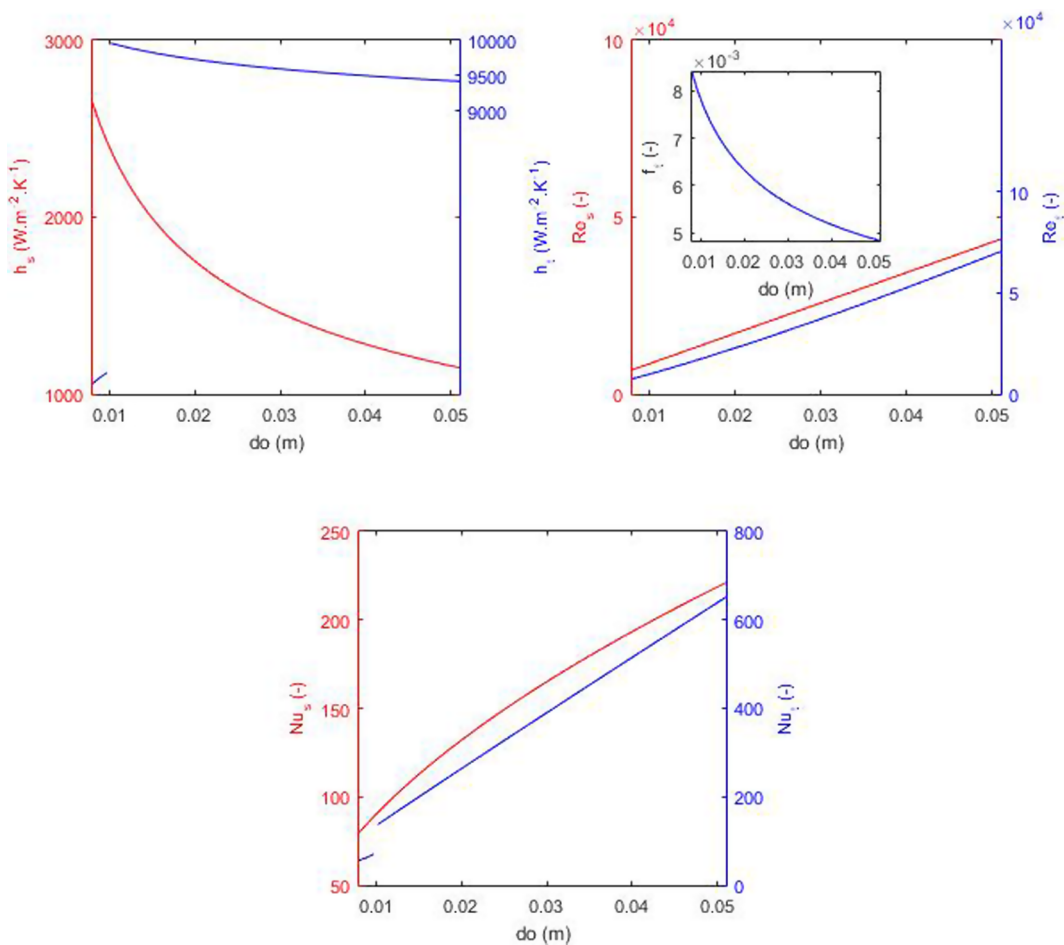


Fig. 11. Variation of the outside tube diameter d_o in limit range and its influence in convective heat transfer coefficients, Reynolds and Nusselt numbers for the shell side for the shell-and-tube heat exchanger study case 1 (red line for shell side and blue line for tube side). The discontinuity of the curves for the convective heat transfer coefficient and Nusselt number for tube side are consistent to the flow regime changes for the shell-and-tube heat exchanger model adopted.

$$A_s = DsB \left(1 - \frac{d_o}{St} \right) \quad (20)$$

The tube side Prandtl number for tube (Pr_t) and shell (Pr_s) sides are determined by,

$$Pr_t = \frac{\mu_t C_p_t}{k_t} \quad (21)$$

$$Pr_s = \frac{\mu_s C_p_s}{k_s} \quad (22)$$

The overall heat transfer coefficient can be determined by,

$$U = \frac{1}{\frac{1}{h_s} + Rf_s + \left(\frac{d_o}{d_i} \right) \left(Rf_t + \frac{1}{h_t} \right)} \quad (23)$$

The logarithmic mean temperature is obtained from,

$$\Delta T_{LM} = \frac{(T_{hi} - T_{co}) - (T_{ho} - T_{ci})}{\ln \left(\frac{T_{hi} - T_{co}}{T_{co} - T_{ci}} \right)} \quad (24)$$

The correction factor is given by,

$$F = \sqrt{\frac{R^2 + 1}{R - 1}} \frac{\ln \left(\frac{1 - P}{1 - PR} \right)}{\ln \left(\frac{2 - PR + 1 - \sqrt{R^2 + 1}}{2 - PR + 1 + \sqrt{R^2 + 1}} \right)} \quad (25)$$

where R is the correction coefficient, and P is the efficiency, are determined, respectively, by,

$$R = \frac{T_{hi} - T_{ho}}{T_{co} - T_{ci}} \quad (26)$$

$$P = \frac{T_{co} - T_{ci}}{T_{hi} - T_{ci}} \quad (27)$$

The heat exchanger surface area is given by,

$$A = \frac{Q}{UF \Delta T_{LM}} \quad (28)$$

For sensible heat transfer, the rate of heat transfer is determined by,

$$Q = \dot{m}_h C_p_h (T_{hi} - T_{ho}) = \dot{m}_c C_p_c (T_{co} - T_{ci}) \quad (29)$$

The tube length is obtained from,

$$L = \frac{A}{\pi d_o Nt} \quad (30)$$

The total annual cost C_{tot} is considered as the objective function, including capital investment (C_i), energy cost (C_e), annual operating cost (C_o), and the total discounted operating cost (C_{od}).

$$C_{tot} = C_i + C_{od} \quad (31)$$

The capital investment cost is determined as a function of the heat exchanger surface area according to,

$$C_i = 8000 + 259.2 A^{0.91} \quad (32)$$

for heat exchangers made with stainless steel for both, shell and tubes.

The total discounted operating cost is determined as a function of

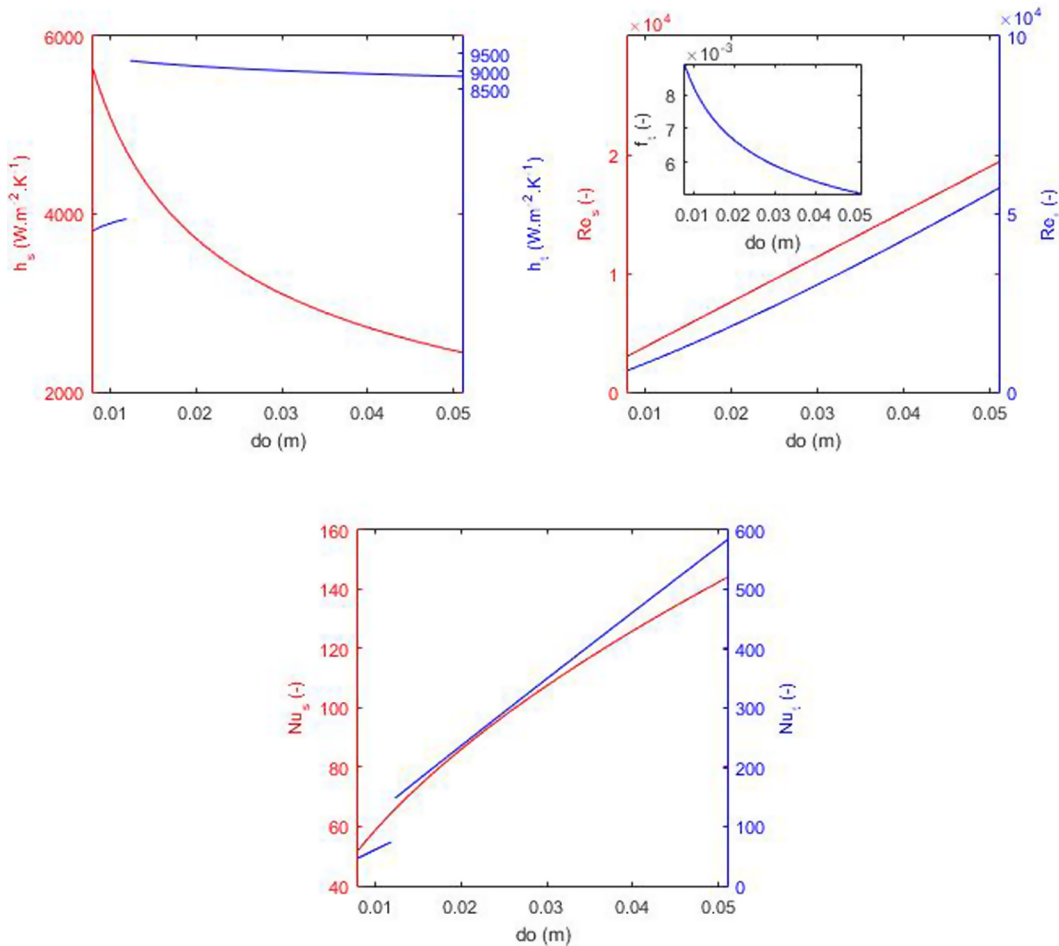


Fig. 12. Variation of the outside tube diameter d_o in limit range and its influence in convective heat transfer coefficients, Reynolds and Nusselt numbers for the shell side for the shell-and-tube heat exchanger study case 2 (red line for shell side and blue line for tube side). The discontinuity of the curves for the convective heat transfer coefficient and Nusselt number for tube side are consistent to the flow regime changes for the shell-and-tube heat exchanger model adopted.

Table 6

Plate-fin heat exchanger inputs and physical properties of the fluids for two case studies.

Parameter	Case 1		Case 2	
	Hot fluid	Cold fluid	Hot fluid	Cold fluid
\dot{m} (kg/s)	1.66	2	25.4	25
T_i (°C)	900	200	460	300
P_i (kPa)	160	200	100	900
C_p (J/kg K)	1122	1073	1060	1060
ρ (kg/m³)	0.6296	0.9638	0.54	4.86
μ (Ns/m²)	0.0000401	0.0000336	0.000032	0.000032
P_f	0.731	0.694	0.69	0.69

the pressure drops for shell and tube sides as,

$$Cod = \sum_{j=1}^{ny} \frac{Co}{(1+i)^j} \quad (33)$$

$$Co = P_p Ce H_{ot} \quad (34)$$

$$P_p = \frac{1}{\eta} \left(\frac{\dot{m}_t}{\rho_t} \Delta P_t + \frac{\dot{m}_s}{\rho_s} \Delta P_s \right) \quad (35)$$

where Ce , H_{ot} , i , and η are the energy cost, the amount of annual work hours, the annual discount rate and the pumping efficiency, respectively.

Table 7

Optimal geometries and thermal properties of the plate-fin heat exchanger case study 1.

Parameter	Original design [56]	GA [34]	ICA [34]	BA [37]	FOA
L_h (m)	0.3	0.95	1	0.997	0.900
L_c (m)	0.3	0.44	0.88	0.940	1
H (mm)	2.49	7.2	5	8.33	8.6
n (fins/m)	782	417	240	257.02	265.2
t (mm)	0.10	0.1	0.19	0.166	0.1
l (mm)	3.18	7.2	9.6	9.51	7.2
N_h	167	57	77	56	53
ΔP_h (kPa)	9.34	4.2	1.23	0.741	0.656
ΔP_c (kPa)	6.90	0.52	0.67	0.460	0.589
L_{noflow} (m)	1	0.87	0.87	0.997	0.976
ε	—	0.821	0.821	0.826	0.827
N_s	0.1576	0.1416	0.1374	0.1341	0.1333

Best result is in bold font.

The shell and the tube pressure drops are given by,

$$\Delta P_s = 1.44 Re_s^{-0.15} \left[\left(\frac{\rho_s v_s^2}{2} \right) \left(\frac{L}{B} \right) \left(\frac{Ds}{de} \right) \right] \quad (36)$$

$$\Delta P_t = \frac{\rho_t v_t^2}{2} \left(\frac{L}{d_t} f_t + 4 \right) n \quad (37)$$

where f_s is the friction factor. Important to notice that the tube side pressure drop is computed as the sum of the distributed pressure drop

Table 8

Optimal geometries and thermal properties of the plate-fin heat exchanger case study 2.

Parameter	Original design [57]	BA [37]	FOA
L_h (m)	0.9	1.654	1.525
L_c (m)	1.8	2.99	3.00
H (m)	0.0057	0.00572	0.01000
t (m)	0.00015	0.000169	0.000100
n (fins/m)	500	388.9	514
l (m)	0.006	0.00857	0.0097
N_h	149	175	94
ΔP_h (kPa)	15	7.5	7.491
ΔP_c (kPa)	10	3.38	3.727
L_{noflow} (m)	1.79	1.99	1.983
ε	0.778	0.83	0.8558

Best result is in bold font.

along the tube length and concentrated pressure losses in elbows as well as in the inlet and outlet nozzles.

3.2.2. Plate-fin heat exchanger

The thermal modelling for the plate-fin heat exchanger was taken from [36], where the Fig. 4a presents the typical arrangement of this type of heat exchanger and Fig. 4b shows its geometrical parameters.

Considering a cross-flow plate-fin heat exchanger with both fluids unmixed, the heat transfer rate is calculated by,

$$Q = \varepsilon C_{min} (T_{hi} - T_{ci}) \quad (38)$$

where ε is the effectiveness, C_{min} is the minimum heat capacity rate and T_{hi} and T_{ci} are the inlet temperatures of the hot and cold fluids, respectively.

The effectiveness is given by [50],

$$\varepsilon = 1 - e^{\left(\frac{1}{Cr}\right)NTU^{0.22}(e^{(-CrNTU^{0.78})}-1)} \quad (39)$$

where $Cr = C_{min}/C_{max}$ and NTU is the number of transfer units determined from,

$$\frac{1}{NTU} = C_{min} \left(\frac{Aff_h}{j_h C p_h Pr_h^{-0.667} \dot{m}_h A_h} + \frac{Aff_c}{j_c C p_c Pr_c^{-0.667} \dot{m}_c A_c} \right) \quad (40)$$

where Aff is the free flow area, A is the heat transfer area, j is the Colburn factor, Cp is the specific heat and Pr is the Prandtl number for each fluid, hot and cold.

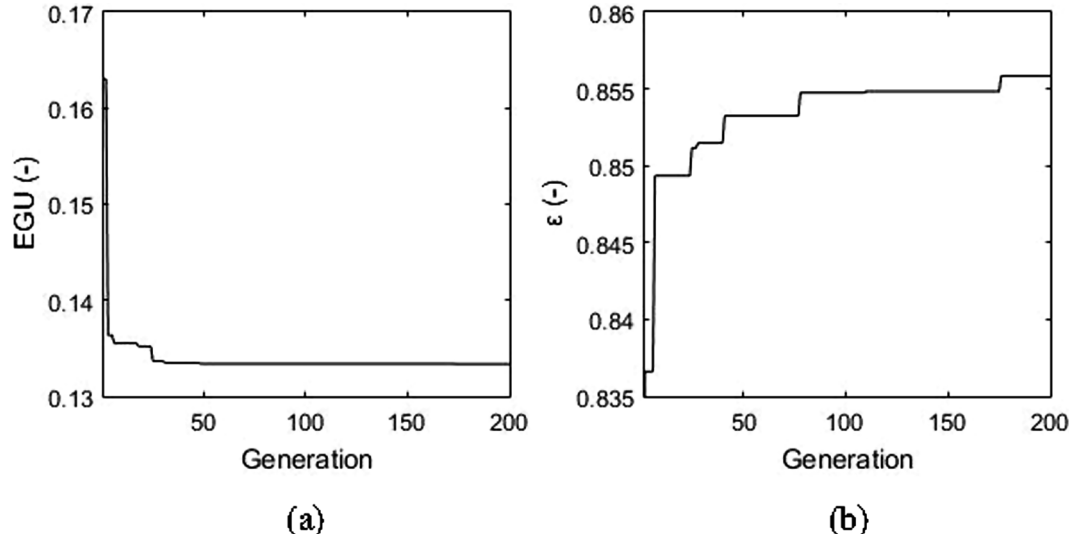


Fig. 13. Convergence rate of the best simulation obtained by FOA for the plate-fin heat exchanger study (a) case 1 and (b) case 2.

The free flow areas can be obtained from,

$$Aff_h = (H_h - t_h)(1 - n_h t_h)L_c N_h \quad (41)$$

$$Aff_c = (H_c - t_c)(1 - n_c t_c)L_h N_c \quad (42)$$

where H is the height of the fin, t is the fin thickness, n is the fin frequency, L is the heat exchanger length and N is the number of fin layers for each fluid, remembering that $N_c = N_h + 1$.

The heat exchangers areas are given by,

$$A_h = L_h L_c N_h (1 + (2n_h(H_h - t_h))) \quad (43)$$

$$A_c = L_h L_c N_c (1 + (2n_c(H_c - t_c))) \quad (44)$$

where the total heat exchanger area $A_{tot} = A_h + A_c$.

The Colburn and Fanning friction factors are determined by [51],

$$j = 0.6522(Re)^{-0.5403}(\alpha)^{-0.1541}(\delta)^{0.1499}(\gamma)^{-0.0677} [1 + 5.3 \times 10^{-5}(Re)^{1.34}(\alpha)^{0.504}(\delta)^{0.456}(\gamma)^{-1.055}]^{0.1} \quad (45)$$

$$f = 9.6243(Re)^{-0.7422}(\alpha)^{-0.1856}(\delta)^{0.3053}(\gamma)^{-0.2659} [1 + 7.7 \times 10^{-7}(Re)^{4.429}(\alpha)^{0.920}(\delta)^{3.767}(\gamma)^{0.236}]^{0.1} \quad (46)$$

where Re is the Reynolds number, $\alpha = s/(H - t)$, $\delta = t/l$, $\gamma = t/s$ and the fin spacing $s = (1/n) - t$ for hot and cold fluids.

The Reynolds number for each fluid of the system can be obtained from,

$$Re = \frac{\dot{m}dh}{Aff\mu} \quad (47)$$

where m is the mass flow rate and μ is the viscosity of each fluid, remembering that $G = \dot{m}/Aff$.

The hydraulic diameter can be determined for both fluids by,

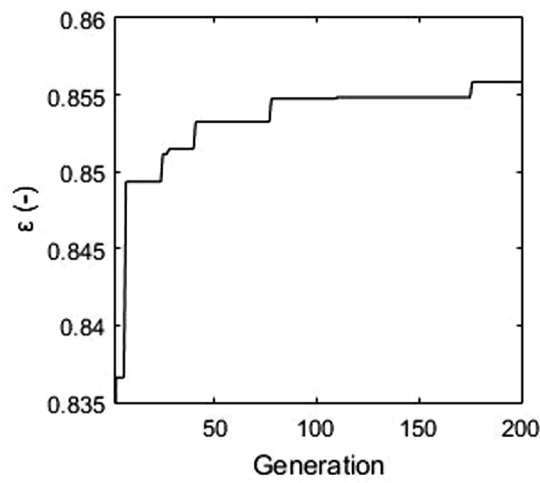
$$dh = \frac{4s(H - t)l}{2(sl + (H - t)l + t(H - t)) + ts} \quad (48)$$

Also, the frictional pressures drop for the two streams is given by,

$$\Delta P = \frac{2fL\left(\frac{\dot{m}}{Aff}\right)^2}{\rho dh} \quad (49)$$

for each one of the fluids.

The convective heat transfer coefficient for both fluids can be



determined by,

$$h = jCpPr^{\frac{-2}{3}} \frac{\dot{m}}{Aff} \quad (50)$$

The no flow length was computed by,

$$L_{noflow} = H - 2t_p + N_h(2H + 2t_p) \quad (51)$$

where t_p is the plate thickness, considered constant equals to 0.005 m.

The outlet pressures and temperatures for both fluids are given by,

$$P_{ho} = P_{hi} - \Delta P_h \quad (52)$$

$$P_{co} = P_{ci} - \Delta P_c \quad (53)$$

$$T_{ho} = T_{hi} - \left(\varepsilon \frac{C_{min}}{C_{max}} (T_{hi} - T_{ci}) \right) \quad (54)$$

$$T_{co} = T_{ci} + \left(\varepsilon \frac{C_{min}}{C_{max}} (T_{hi} - T_{ci}) \right) \quad (55)$$

The objective function is defined as the entropy generation units, that is given by Bejan [52],

$$Ns = (1 - \varepsilon) \left[\frac{(T_{ci} - T_{hi})^2}{T_{ci} T_{hi}} \right] + \left(\frac{Rcte_h}{Cp_h} \right) \left(\frac{\Delta P_h}{P_{hi}} \right) + \left(\frac{Rcte_c}{Cp_c} \right) \left(\frac{\Delta P_c}{P_{ci}} \right) \quad (56)$$

valid for $(1 - \varepsilon) \ll 1$ and $\left(\frac{\Delta P}{P} \right) \ll 1$, where $Rcte$ is the specific gas constant.

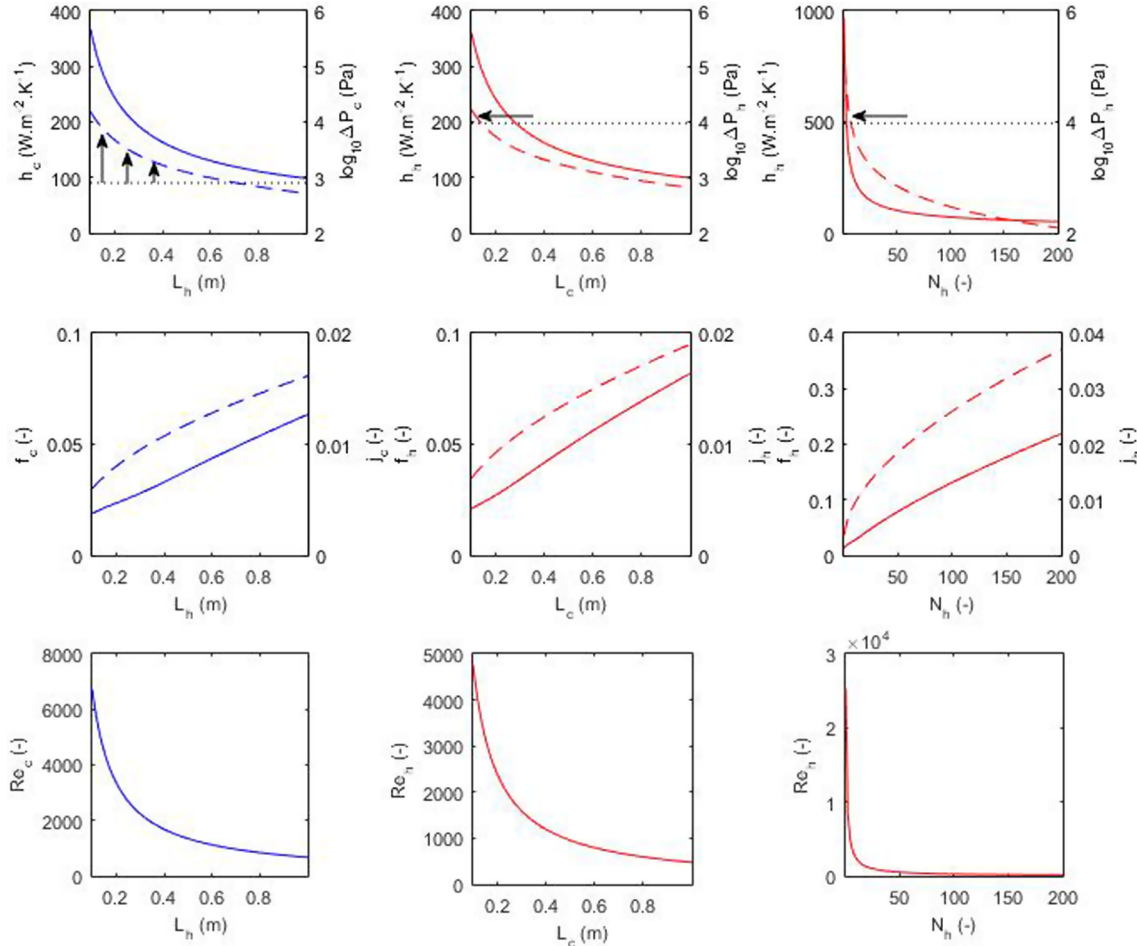


Fig. 14. Variation of the lengths for hot (L_h) and cold fluids (L_c) and number of hot layers (N_h) in limit range and its influence in convective heat transfer coefficients, pressure drops, Colburn and Fanning friction factors and Reynolds numbers for the plate-fin heat exchanger study case 1 (continuous line for left y axis and dashed line for right y axis). The dotted lines and arrows indicate the fraction of the curve that are violating the constraint for the cold stream pressure drop for L_h and for the hot stream pressure for L_c and N_h .

4. Results and discussion

The following subsections present the results obtained with the simulations for both single-objective benchmark functions and heat-exchanger cases. For the single-objective function the comparison algorithms were set as follows: Genetic Algorithm (GA) (crossover and mutation probabilities equals to 0.9 and 0.001, respectively), Particle Swarm Optimization (PSO) (cognitive and social constants equals to 2 and inertia weight equals to 0.5), Bat Algorithm (BA) (both loudness and pulse rate equals to 0.5) and Firefly Algorithm (FA) (α , β_{min} and γ equals to 0.5, 0.2 and 1, respectively). For better understanding of the comparison algorithms the authors suggest consulting the references [11,12,53,54].

4.1. Single-objective benchmark problems

The results for the benchmark single-objective optimization are shown in Table 2 alongside to its average and standard deviations values and average processing time.

It can be observed in Table 2 that the proposed algorithm obtained best values for eleven of the twelve benchmark functions tested (f_1 to f_9 , f_{11} and f_{12}), outcoming GA, PSO, BA and FA. The function f_{10} was better optimized by GA followed by FOA and the function f_{11} was optimized for all comparison algorithms alongside FOA. However, despite the performance of the proposed technique, FOA reached processing time as high as PSO. The pairwise comparison between FOA and each one of

the other algorithms evaluated for the benchmark functions using the Wilcoxon ranksum test over all simulations suggest that the proposed algorithm has statistically significant superiority and that the results do not come from the same population.

Another situation that may be emphasized is the possible reason why FOA did not perform better in all multimodal function (the exception is the f_{10} function). This may be associated to the mechanism of selection of random chosen candidates to perform the logarithmic spiral and dive motions, that mostly promotes exploration of the search space and take more generations to local optima avoidance. Considering the results obtained for some functions, new simulations ($D = 2$, $NP = 5$, $iter_{max} = 100$) were performed where the results were evaluated for the search history, convergence rate and average fitness for each generation population (Fig. 5).

In this case the first metric has qualitative character, showing the history of sampled points over the generations progress (black points) until the best value obtained (red point). The plots show that FOA may explore the search space and exploit the surroundings of the global optima with high accuracy. The second and third metrics have quantitative character, where the average fitness over the generation progress is clearly improved and the convergence rate shows high acceleration to the global optima.

4.2. Shell-and-tube heat exchanger optimization

Two case studies to shell-and-tube heat exchanger were used. The lower and upper bounds adopted in both studies were the shell internal diameter (D_s) ranging from 0.2 m to 1.0 m, the tubes outside diameter (d_o) ranging from 0.008 m to 0.051 m and baffles spacing (B) ranging from 0.2 m to 0.5 m. The objective function was computed for the total discounted operating costs with $ny = 10$ years, $Ce = 0.00012$, $H_{ot} = 7000$, $i = 0.1$, and $\eta = 0.8$.

The first case study for shell-and-tube heat exchanger was presented by Sinnott [49] where a system for thermal exchanging with two tube passages and one shell passage for methanol and brackish water, with 4.43 MW of heat duty, have to be optimized for minimum total cost. The second case, described in Table 3, consists in the application from Kern [55] where a heat exchanger with two tube passages and one shell passage for distilled water and raw water, with 0.46 MW heat duty, have to be designed also for minimum total cost. The parameters inputs and physical properties of the fluids are presented in Table 3 for both cases.

The results, in the first case study, for the shell-and-tube optimization aiming the minimization of the total annual cost were compared with the works of Sinnott et al. [49], Caputo [21] (GA), Patel & Rao

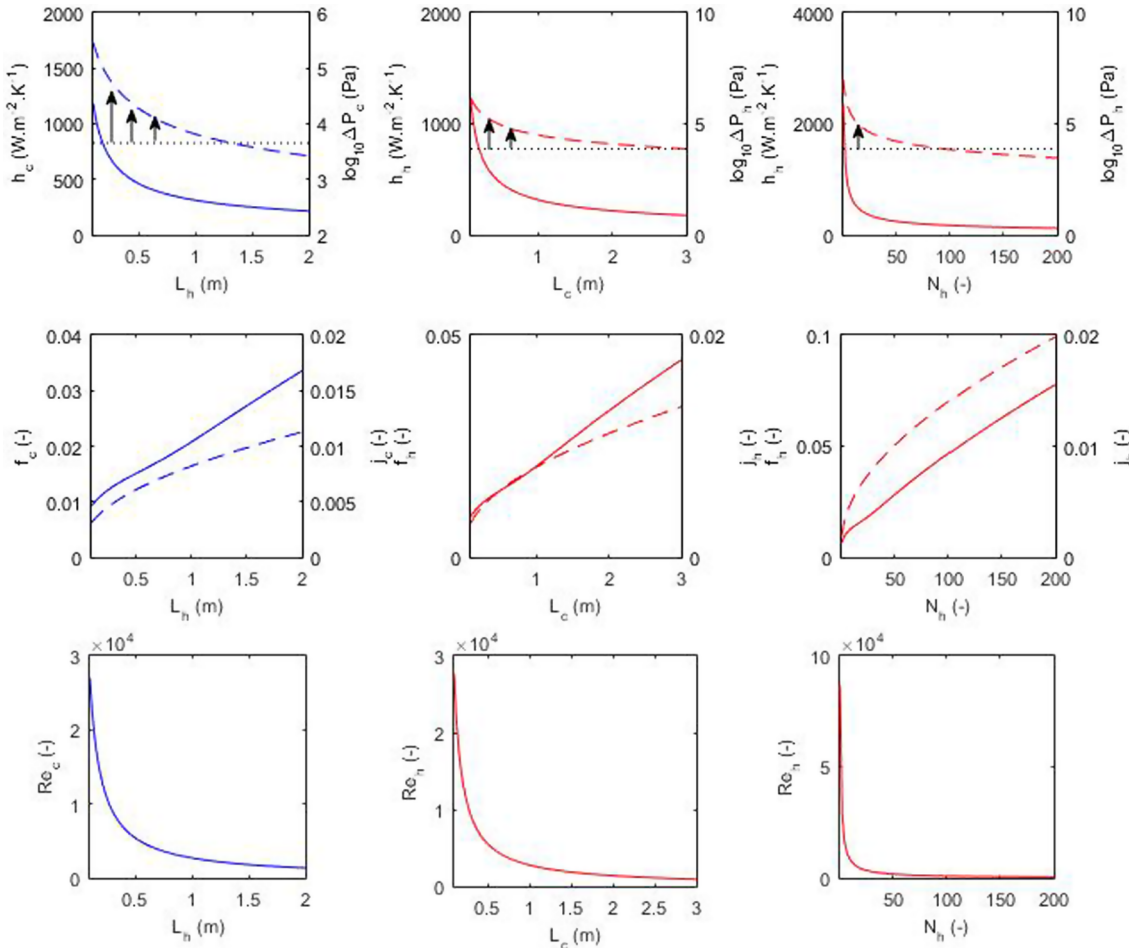


Fig. 15. Variation of the lengths for hot (L_h) and cold fluids (L_c) and number of hot layers (N_h) in limit range and its influence in convective heat transfer coefficients, pressure drops, Colburn and Fanning friction factors and Reynolds numbers for the plate-fin heat exchanger study case 2 (continuous line for left y axis and dashed line for right y axis). The dotted lines and arrows indicate the fraction of the curve that are violating the constraint for the cold stream pressure drop for L_h and for the hot stream pressure for L_c and N_h .

[23] (PSO), Hadidi et al. [26] (ICA), Hadidi et al. [25] (BBO), Sahin et al. [24] (ABC) and Asadi et al. [13] (CSA). It can be observed in Table 4 in comparison to the original study [54] that a reduction of 28% was obtained, while decreases for the variables D_s and d_o and an increase in B were achieved. Also, increasing in heat transfer coefficients for both fluids were obtained. Considering a more recent case [13], a reduction about 2.5% was obtained for total cost and the same behavior about the decision variables were observed in relation to the original case study (reduction of 17.41% in D_s , 33.11% in d_o and increase of 20.77% in B). However, both heat transfer coefficients and pressure drop for tube side increased their respective values.

Even if FOA achieved better total cost value, it presented higher operational cost, due to the pressure drops obtained. It is important to notice that reduction in the heat exchanger length lead to a decreasing in the heat exchanger surface transfer area, notwithstanding the number of tubes and the outside diameter of the tubes present increase and decrease, respectively. Yet, increasing in the number of tubes and decreasing in the shell diameter provide lower flow velocities, directly linked to the pressure drops.

In the second case study the optimization also aimed the minimization of the total cost and the results presented in Table 5 are compared with the original design [55], Caputo et al. [21] (GA), Patel & Rao [23] (PSO), Sahin et al. [24] (ABC) and Hadidi & Nazari [25] (BBO). Comparing the results obtained with FOA against those ones presented in the original case study [55] a reduction of 57.8% was achieved alongside increasing in shell diameter and baffles spacing and for the tube side heat transfer coefficient, while decreasing were reached for both tube and shell pressure drops and for the shell side heat transfer coefficient. About a newer work [25], the difference between the values for the total cost differs 3.9% favoring FOA. Also, FOA presented D_s with a lower value (6.8%) and d_o variable with a higher value (20%, respectively) while B did not changed. In this case, shell side heat transfer coefficients and pressure drop reached lower values than the ones presented by [25] (4.65% and 6.7% respectively) while for tube heat transfer coefficients and pressure drop achieved higher values (1.5% and 9.9% respectively).

For the second case of shell-and-tube heat exchanger, the increase in the shell diameter and number of tubes lead to a reduction of the

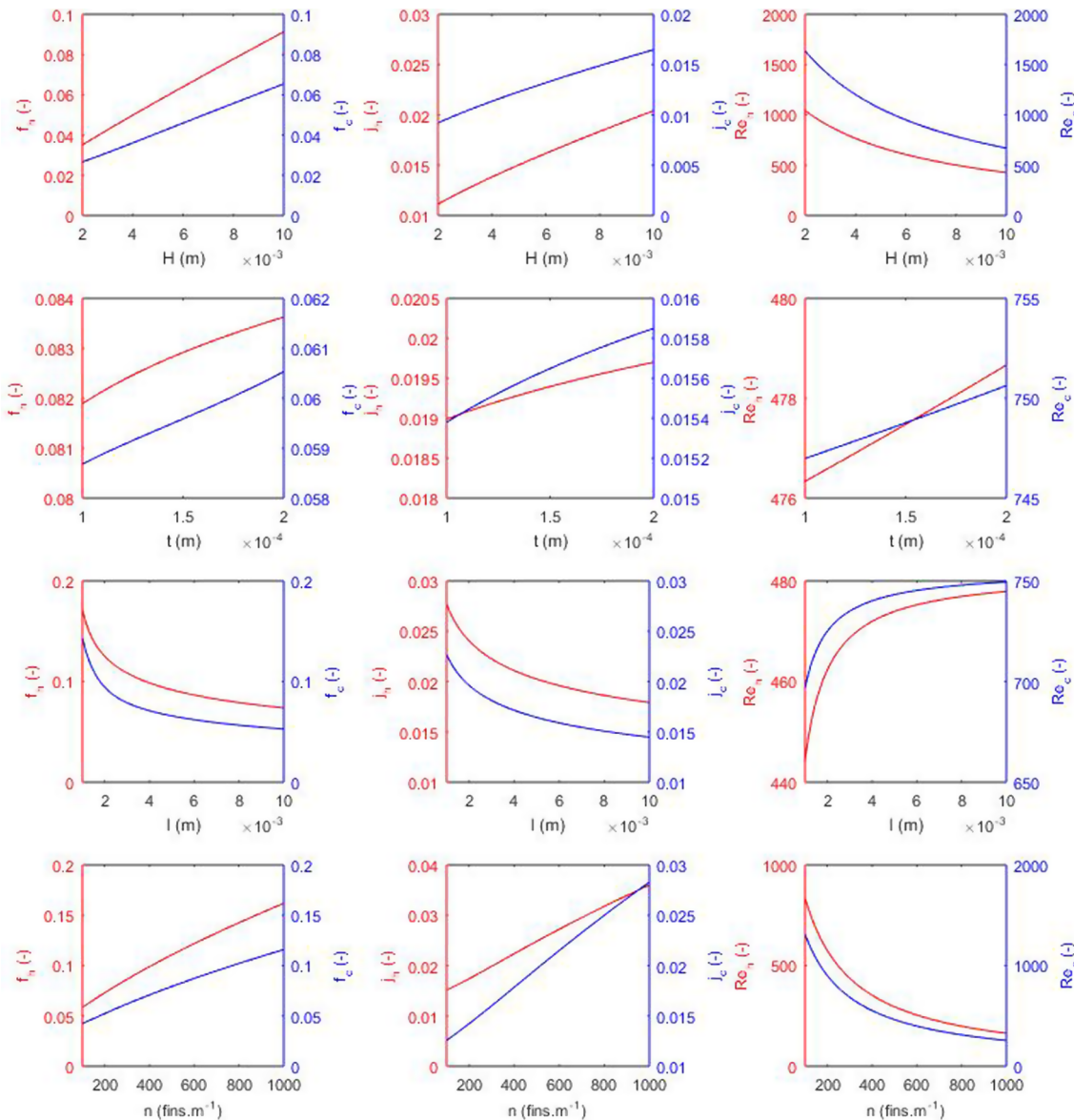


Fig. 16. Variation of the fin geometrical parameters (H , t , l and n) in limit range and its influence in Colburn and Fanning friction factors and Reynolds numbers for the plate-fin heat exchanger study case 1 (red line for hot fluid and blue line for cold fluid).

investment cost, since they provide changes in the heat exchanger length and heat exchangers surface transfer area. It is important to notice that, similarly to first case study, reductions in the flow velocities culminate in impacts over the pressure drops, making the operational cost increase, even if compensated later with the decreasing in the investment cost.

The convergence rate for cases 1 and 2 applying FOA are shown in Fig. 6a and b, respectively, where the best values are reached after 120 generations for case 1 and 180 generations for case 2, respectively.

For both shell-and-tube heat exchangers optimization aiming total cost minimization, despite the best results obtained by FOA higher values for the operational cost (linked to the pressure drops) were observed, compensated by lower investment costs related directly to the heat exchanger area.

Yet, a thermal-hydraulic analysis was performed for each variable for both cases, considering the variation of one variable on the limit range while the remaining variables were fixed to the optimization value obtained. The Figs. 7–12 presents the results regarding the

convection heat transfer coefficient, pressure drops and Reynolds and Nusselt numbers.

From the Figs. 7 and 8 it can be observed that higher values for the shell diameter results in lower Reynolds numbers for shell, influenced by the shell diameter in the determination of the cross-sectional area normal to flow direction, and tube, influenced by the shell diameter in the determination of the flow velocity once this parameter is dependent to the number of tubes calculation. This behavior contribute to the decay curves of the convective heat transfer coefficients for shell and tube fluids, which both presents dependency with the Reynolds numbers, Nusselt numbers (directly dependent of the convection heat transfer coefficients) and pressure drops, where for the shell exist explicit dependency with the shell diameter (where there is also contribution by the Reynolds number and length of the heat exchanger, this last by the inverse relation of the number of tubes). Yet, the decay in the Reynolds number for tube side results in an increase on the respective friction factor.

Regarding the baffles spacing (Figs. 9 and 10), the model reveals

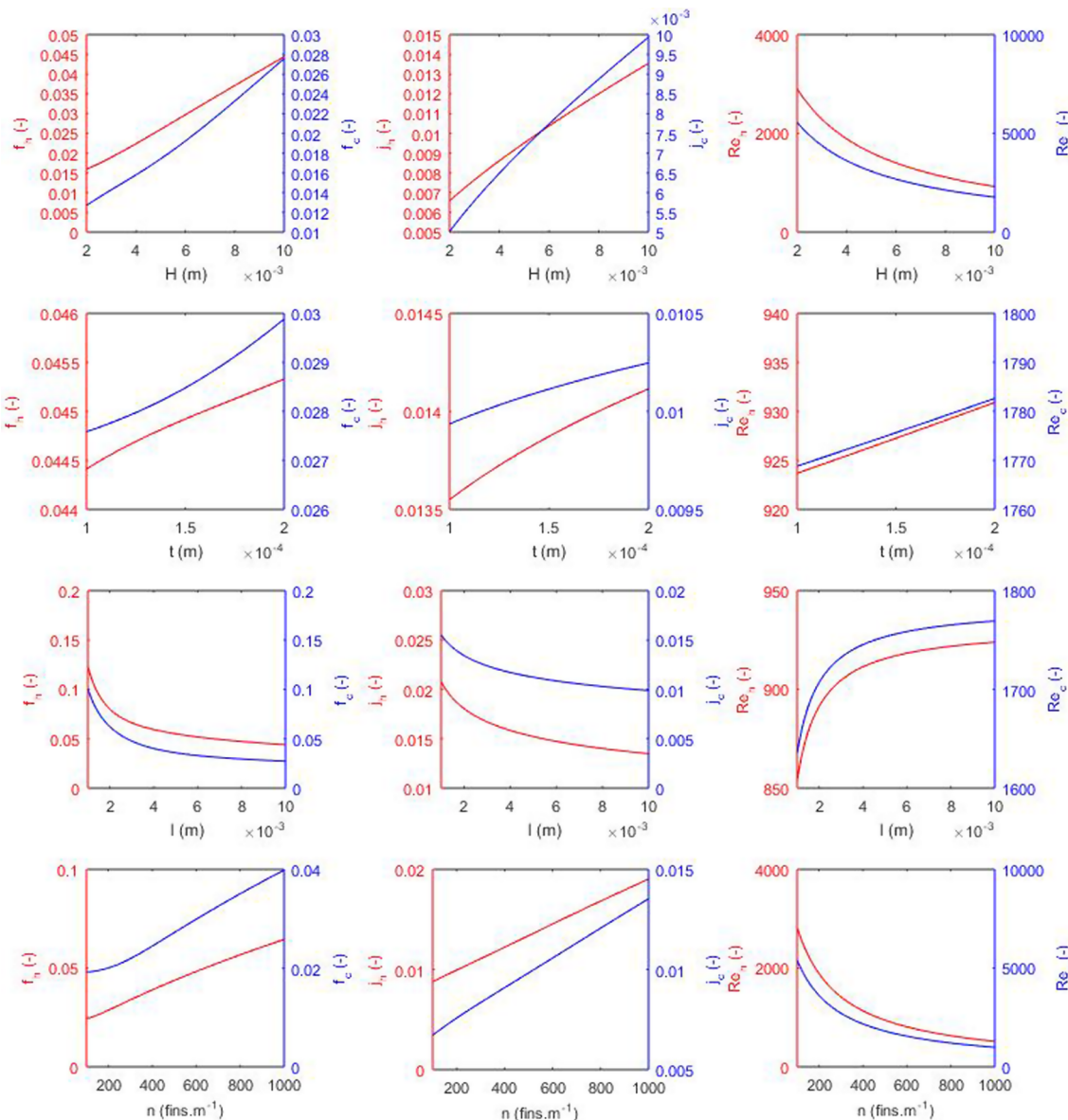


Fig. 17. Variation of the fin geometrical parameters (H , t , l and n) in limit range and its influence in Colburn and Fanning friction factors and Reynolds numbers for the plate-fin heat exchanger study case 2 (red line for hot fluid and blue line for cold fluid).

that this variable presents influence in the shell side about the Reynolds number (higher values lead to lower Reynolds numbers), by the determination of the cross-sectional area normal do the flow direction, resulting in a decay behavior of the convective heat transfer coefficient and in the pressure drop (where exist also an inverse explicit dependency).

About the outside diameter of tubes (Figs. 11 and 12) there is a dependency of the that variable with the Reynolds numbers for both shell and tube sides, the first by the determination of the internal diameter of tubes and the second by the equivalent diameter. An increase in the outside diameter of tubes lead to higher Reynolds Numbers, impacting in the convective heat transfer coefficient where a decay behavior is obtained both shell and tube sides, including the variation in the convective heat transfer coefficient for the tube side regarding the mathematical model and its dependency with the Reynolds number and the flow regime. This behavior also impacts the Nusselt numbers of the fluids.

In general, for case study 1 and 2, despite the decay curve for the Reynolds numbers for the shell diameter and baffles spacing the flow regime tend to be maintained turbulent, leaving this situation only for values of shell diameter and baffle spacing very close to the upper limit range. For the outside tube diameter also corroborates the previous affirmation about the flow regime once its increase only causes augmentation of the Reynolds numbers values (even in the lower limit range, the Reynolds numbers obtained are already close to the turbulent flow regime). Also, the results for the Nusselt numbers indicates that the process in the entire range of the variables is based on

convective heat transfer process. Yet, the discontinuity of the curves for the convective heat transfer coefficient, friction coefficient and Nusselt number for tube side and pressure for hot side are consistent to the flow regime changes for the shell-and-tube heat exchanger model adopted.

4.3. Plate-fin heat exchanger optimization

Two plate-fin heat exchangers were tested, and the physical properties of the fluids are presented in Table 6. The first case study for plate-fin heat exchanger was taken from Shah [56], where a gas-to-air single pass cross-flow heat exchanger, with 1069.8 kW of heat duty, have to be designed for minimum entropy generation units with maximum pressure drops of 9500 and 800 Pa for hot and cold fluids, limited to $1 \times 1 \times 1$ m. The second case study investigated is from Kakaç and Liu [57] where a gas-to-air cross flow plate-fin heat exchanger with a requirement heat duty of 3300 kW and air as fluid on both sides has to be designed for maximum effectiveness. The heat exchanger is limited to $2 \times 3 \times 2$ m and the maximum pressure drops for hot and cold fluids are 7.5 kPa and 4.5 kPa, respectively.

For the first case study the lower and upper boundary of the optimization variables were heat exchanger length for hot and cold fluids (L) ranging from 0.1 m to 1.0 m, the height of fin (H) from 0.002 m to 0.01 m, the fin frequency (n) from 100 to 1000, the fin thickness (t) from 0.0001 m to 0.0002 m, the lance length of the fin (l) from 0.001 m to 0.01 m, and the number of fin layers for the hot fluid (N_h) from 1 to 200.

The results for case 1 are presented in Table 7 and were compared

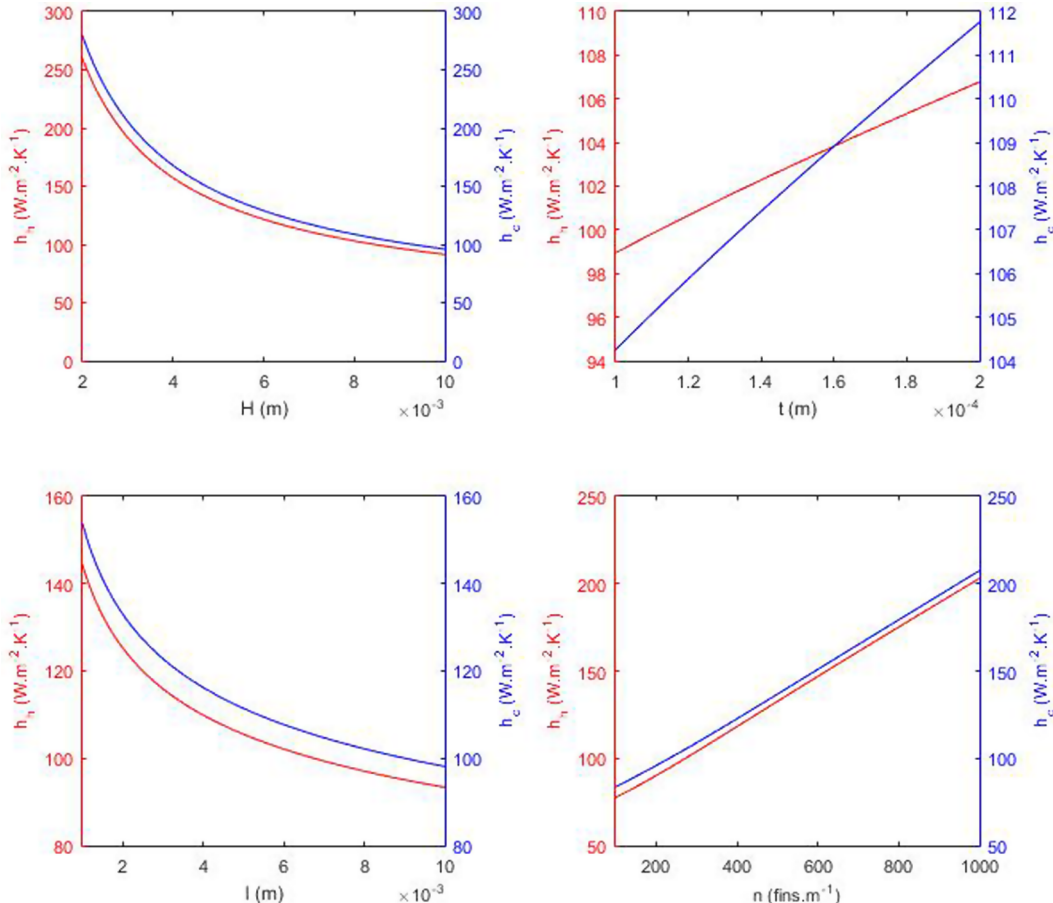


Fig. 18. Variation of the fin geometrical parameters (H , t , l and n) in limit range and its influence in convective heat transfer coefficients for the plate-fin heat exchanger study case 1 (red line for hot fluid and blue line for cold fluid).

with the original design [56] and the works of Yousefi et al. [34] (GA and ICA) and Zarea et al. [37] (BA). It can be observed in comparison to the original study [56] that a reduction of 15.42% was obtained for the objective function, with increases in all decision variables, except n and N_h , pressure drops also presented significant reduction. Considering a more recent work [37], a better value was achieved alongside increases in the decision variables L_c and n , while decreases were observed for the variables L_h , H , N_h , t and l . About the pressure drops an increase of 28% and a decrease of 11.47% for cold and hot fluid streams were obtained, respectively. The optimization achieved better distribution between the pressure drops for hot and cold streams with a lower difference between both results. Also, in comparison to the last recent study the heat exchanger the optimization reached even lower volume (0.8784 m³ for FOA against 0.9343 m³ for BA) and better effectiveness.

For the second case study the results for the gas-to-air plate-fin optimization aiming the maximization of effectiveness were compared with the original design [57] and Zarea et al. [37] (BA), like presented in Table 8. The lower and upper bounds for the optimization variables were the heat exchanger length for hot fluid (L_h) ranging from 0.1 m to 2.0 m, the heat exchanger length for cold fluid (L_c) ranging from 0.1 m to 3.0 m, and the other parameters have the same values that the previous case study. In this case, restrictions about the maximum allowable pressure drops and no flow length were adopted.

Comparing the results, presented in Table 8, obtained with the original case study design [57] an enhancement about 10% for the effectiveness was reached with increases in all the decision variable, except t and N_h . The pressure drops for hot and cold fluid streams also

presented significant decreases while the no flow length reached value closer to the constraint. Now, concerning the recent work [37], alongside the better value obtained for the effectiveness by FOA, increases for the decision variables L_h , H , n and l were achieved while for L_c and N_h decreases were observed. About the pressure drops a slightly reduction is presented for the hot fluid stream and for the cold fluid stream 10.27% of increasing. For the second plate-fin heat exchanger case, it can be observed that increases in the length of the streams lead to increasing in the heat exchangers transfer area, also rising the NTU, impacting the effectiveness of the thermal transfer process.

The convergence rate for FOA is illustrated in Fig. 13a and b, for case 1 and 2, respectively, where can be observed that the optimal value was achieved after 50 generations for both cases.

For the plate-fin heat exchangers case studies, despite the distinct difference in the objective functions adopted, better values were achieved in comparison to the previous studies and original design. Also, fact to be emphasized was the variation of all the decision variables promoted by FOA, suggesting the potential for the space search exploration that the algorithm possesses.

Similarly, to the cases for the shell-and-tube heat exchangers, a thermal-hydraulic analysis for the plate-fin heat exchanger was evaluated considering the all de decision variables. Each variable was varied within the limit range while the remaining variables continued with the optimization value reached. These results are presented in Figs. 14–21 regarding the influence of each variable in the convective heat transfer coefficients, Colburn and Fanning friction factors, Reynolds number, pressure drops and some comments regarding the

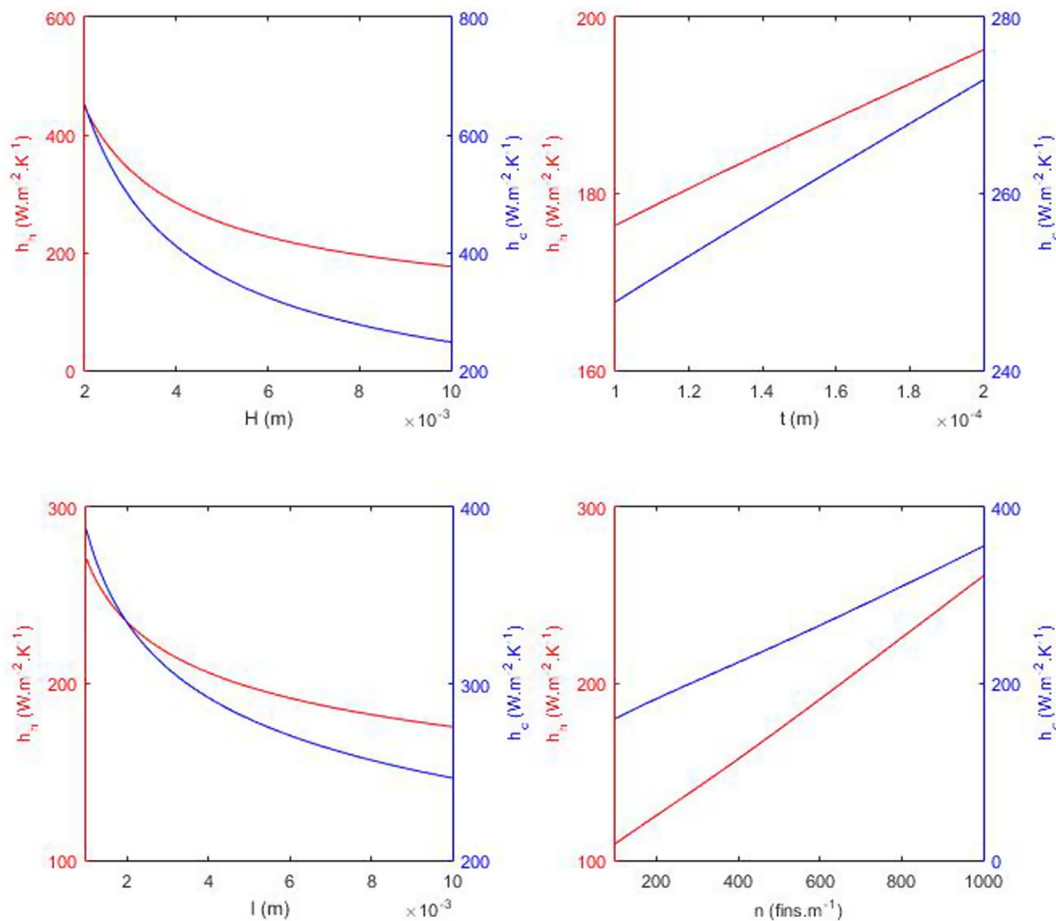


Fig. 19. Variation of the fin geometrical parameters (H , t , l and n) in limit range and its influence in convective heat transfer coefficients for the plate-fin heat exchanger study case 2 (red line for hot fluid and blue line for cold fluid).

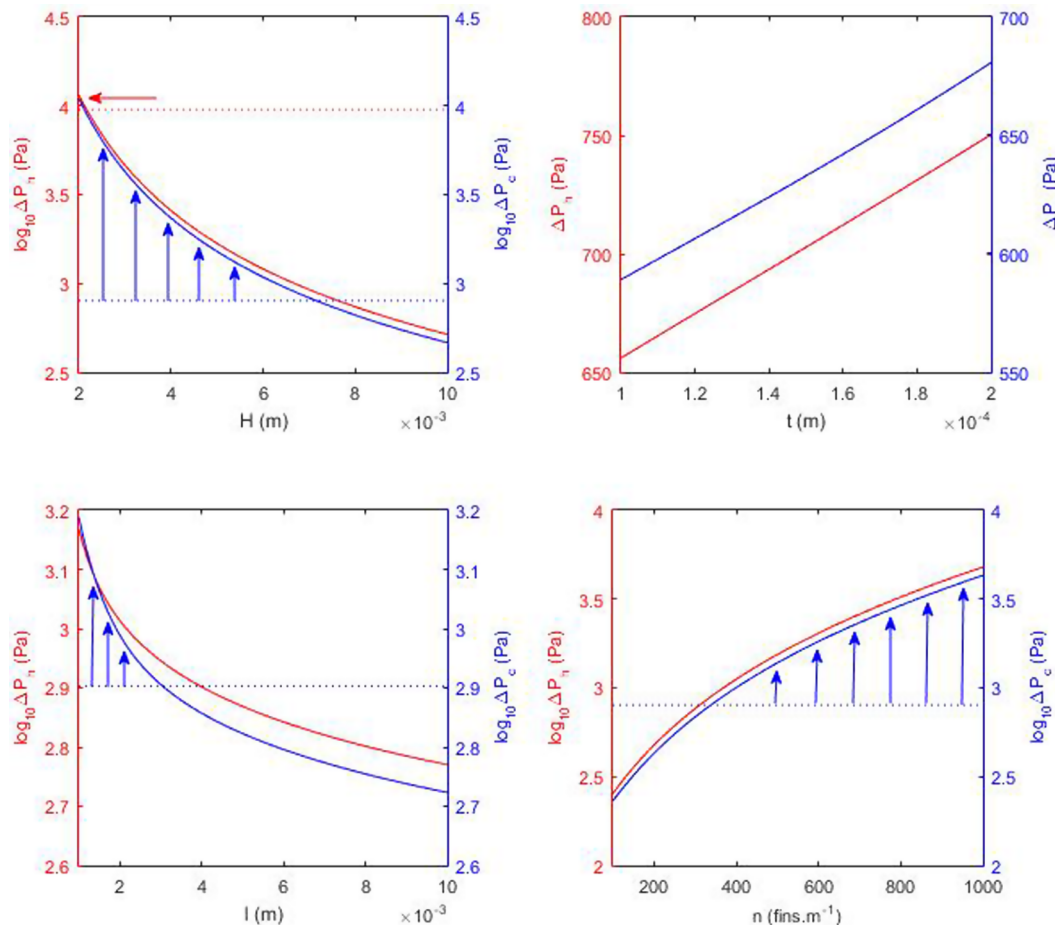


Fig. 20. Variation of the fin geometrical parameters (H , t , l and n) in limit range and its influence in pressure drops for the plate-fin heat exchanger study case 1 (red line for hot fluid and blue line for cold fluid). The blue dotted lines and arrows indicate the fraction of the curve that are violating the constraint for the cold stream pressure drop, while the red dotted lines and arrows indicate the fraction of the curve that are violating the constraint for the hot stream pressure drop.

constraints violation for the pressure drops are presented. Finally, Fig. 22 presents a comparison of the no flow length constraint violation.

First of all, we have to consider that the length of the plate-fin heat exchanger for hot fluid impacts the parameters for the cold one and vice-versa, while the number of hot and cold layers impacts their respective fluid. Explained that we can observe (from Figs. 14 and 15) that greater heat exchanger lengths, no matter if its hot or cold, lead to lower Reynolds numbers once exist dependency of that parameter with the free flow areas.

This fact causes an increasing behavior for the Colburn and Fanning friction factors, where the first influence the convective heat transfer coefficient. Despite this influence, the variation caused by the Colburn factor is weaker of the that caused by the free flow area, culminating in a decay curve for the convective heat transfer coefficient. The Fanning friction factors contributes for the pressure drops, but also not enough to overcome the influence of the free flow areas inverse relation for this parameter.

Similarly, the number of hot layers directly contribute for the free flow area for the hot fluid, decreasing the Reynolds number as its value increases influencing the Colburn and Fanning friction factors, the convective heat transfer coefficients and the pressure drops in an equivalently to the analysis for the lengths of the plate-fin heat exchanger.

The variables related to the fins (Figs. 16 and 17) work primarily on the hydraulic diameter, which influence directly the Reynolds numbers and consequently the Colburn and Fanning friction factors. We may not forget the relations for the fin spacing and geometrical parameters α , δ and γ (where higher H decreases α , higher l decreases δ , higher n decreases s that decreases γ , and higher t decreases α but increases δ , γ and s).

Considering the results for the Colburn factor and those obtained for the convective heat transfer coefficient (Figs. 18 and 19) we can infer that the thickness of the fin has weak of low influence on the convective heat transfer coefficient for both cases.

Similar behavior is observed again for the thickness of the fin for the pressure drops (from Figs. 20 and 21), considering its influence for the Fanning friction factor.

From the analysis presented, some observations may be highlighted, such as that the increases in the lengths of the heat exchanger lead to non-turbulent flow regime. Yet, from the four variables related to the fin geometry those that has greater influence on the convective transfer coefficient are the fin height and density of fins for plate-fin heat exchanger case study 1, and for the plate-fin case study 2 the lance length of the fin may be included in this matter. Also, the variables linked to the fin geometry that present higher variation for the pressure drops are the height of the fin and the density of fins. The thickness of the fin, in

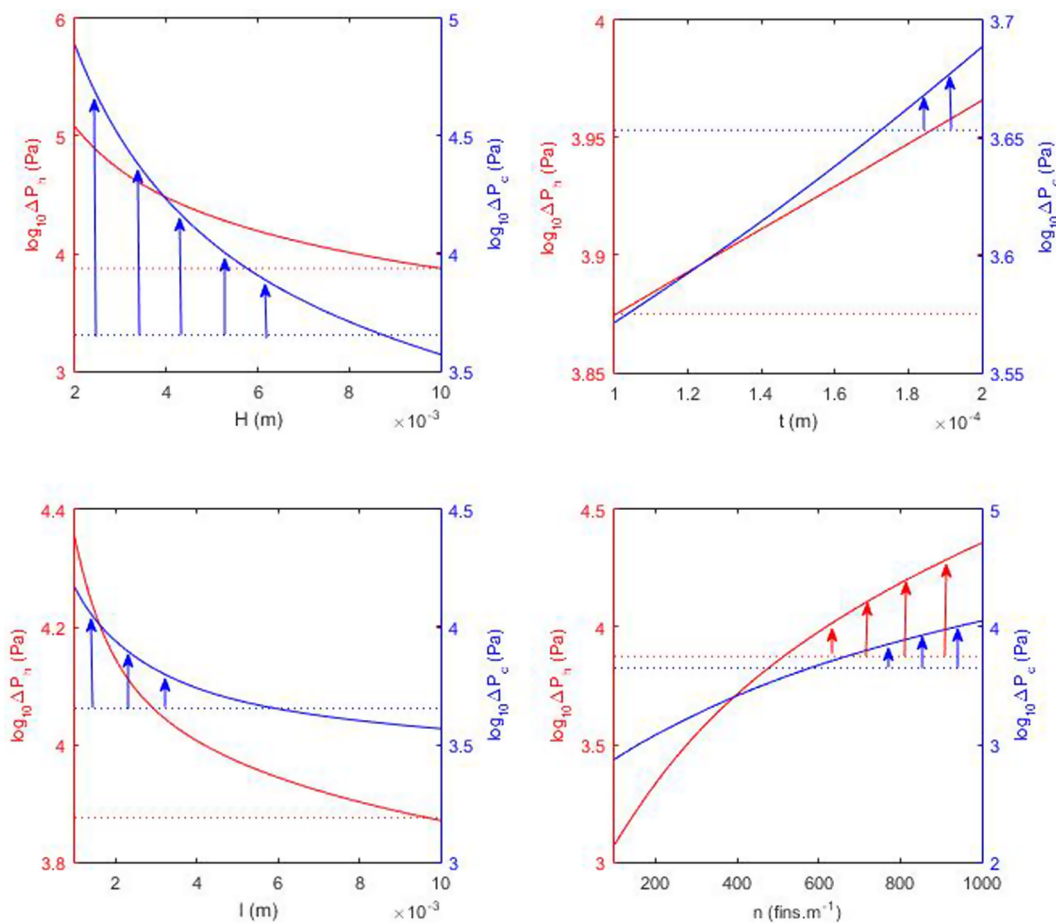


Fig. 21. Variation of the fin geometrical parameters (H , t , l and n) in limit range and its influence in pressure drops for the plate-fin heat exchanger study case 2 (red line for hot fluid and blue line for cold fluid). The blue dotted lines and arrows indicate the fraction of the curve that are violating the constraint for the cold stream pressure drop, while the red dotted lines and arrows indicate the fraction of the curve that are violating the constraint for the hot stream pressure drop.

both cases, presented low influence on the Colburn factor and Fanning friction factor.

Taking account the constraint for pressure drops and no flow length, for the plate-fin case study 1, the pressure drop for cold stream constraint begin to be violated for L_h lower than 0.712 m, H lower than 0.0072 m, l lower than 0.0031 m and n higher than 343 fins/m, while the pressure drop constraint for the hot stream present this issue for L_c lower than 0.145 m, for a very few layers for the hot fluid (less than 9 layers) and H values closer to the lower limit range (0.002 m).

About the plate-fin case study 2, the pressure drop for cold stream constraint begin to be violated for L_h lower than 1.335 m, H lower than 0.0088 m, l for values close to 0.006 m and lower, t close to 0.0017 and higher and n close and superior to 577 fins/m, while the pressure drop constraint for the hot stream present this issue for N_h lower than 94 and n closer and superior to 514 fins/m (for L_c , H , l and t the constraint belong to the limit range achieved in the optimization).

Regarding the no flow length constraint, the case study 1 presents violation for very high values for the height of the fin (superior to 0.0088 m) and for a number of hot layers superior of 55 layers, approximately. For the case study 2 this violation occurs only for values of N_h closer and superior to 93 layers.

5. Conclusion and future research

Based on the hunt behavior of falcons, a novel metaheuristic algorithm, called Falcon Optimization Algorithm (FOA), was proposed in

this paper. FOA is a population-based algorithm that needs the adjustment of few parameters. The results obtained showed that the proposed algorithm reached good results both single-objective, achieving better values against the other algorithm tested (GA, PSO, BA and FA) with competitive time processing. Considering the results achieved in the single-objective optimization the novel proposed technique it was applied in heat exchangers shell-and-tube and plate-fin types, obtaining better results than previous works for the objective functions total cost for shell-and-tube heat exchanger (28% and 57.8% of reduction for cases 1 and 2, respectively) and number of entropy generation units (15.42% of reduction for case 1) and effectiveness (10% of increase for case 2) for plate-fin heat exchanger type. Also, the simulations suggested the great potential that FOA has to explore de space search for distinct variables, continuous or discrete. Also, the thermal-hydraulic analysis was able to provide the influence of each variable about convective heat transfer coefficients, pressure drops, Reynolds and Nusselt numbers and friction coefficient for the shell-and-tube heat exchangers, and for the plate-fin heat exchangers about the convective heat transfer coefficients, pressure drops, Colburn and Fanning friction factors and Reynolds numbers and constraints violation.

For future research multiobjective optimization could be explored under capacity, convergence and diversity point of views for an algorithm with few adjustment parameters, or even self-adjustable parameters, for the Pareto front achievement.

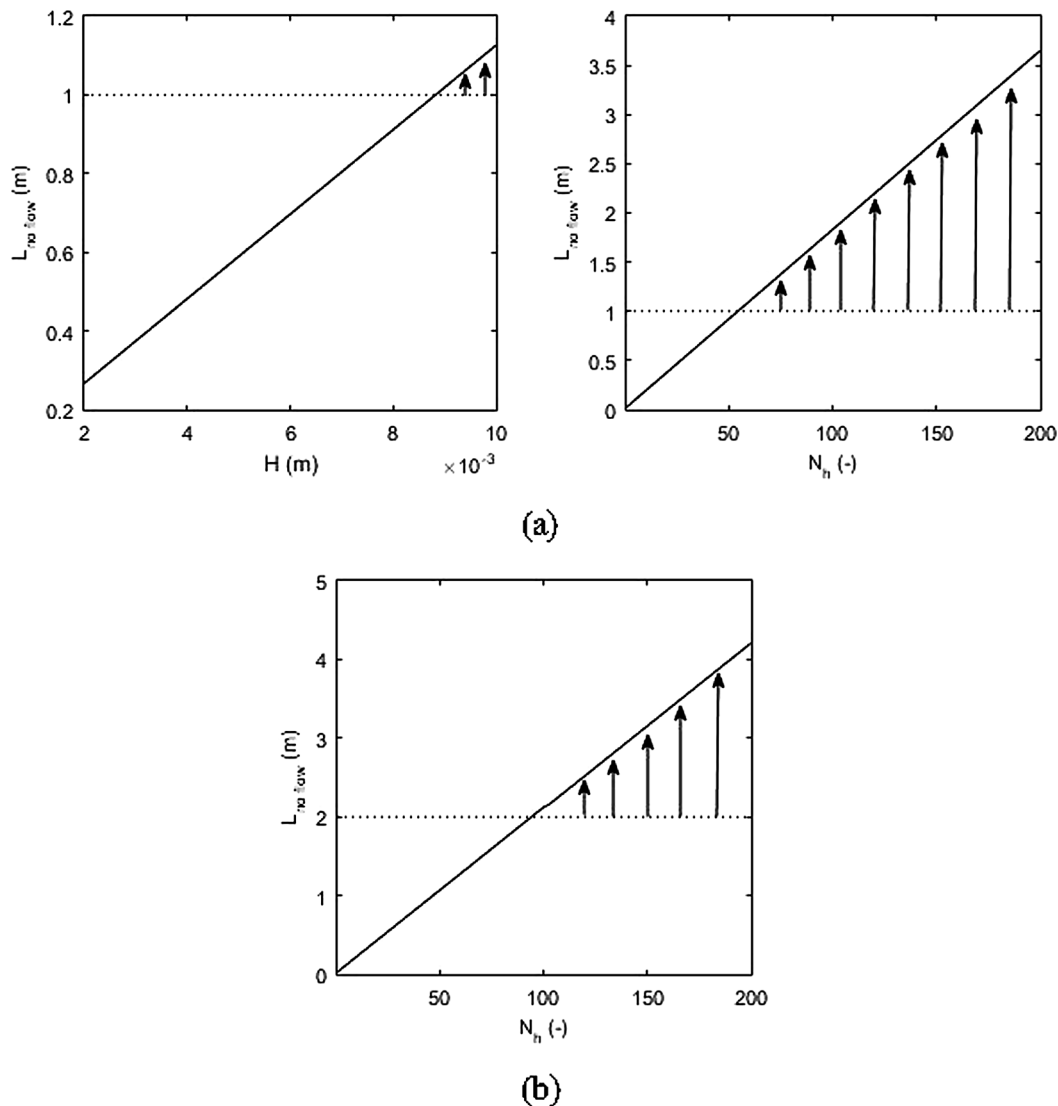


Fig. 22. Violation of the constraint for the no flow length for plate-fin study case 1 (a) and case 2 (b). The dotted lines and arrows indicate the fraction of the curve that are violating the constraint for the no flow length.

Acknowledgements

The authors would like to thank National Council of Scientific and Technologic Development of Brazil - CNPq (grant: 152503/2018-8-PDJ) for the scholarship financial support of this work, and grants: 303908/2015-7-PQ, 303906/2015-4-PQ, 404659/2016-0-Univ, 405101/2016-3-Univ) and Araucaria Foundation (PRONEX – 042/2018) for financial support of this work. Furthermore, the authors wish to thank the Editor and anonymous referees for their constructive comments and recommendations, which have significantly improved the presentation of this paper.

References

- [1] I. Boussaid, J. Lepagnot, P. Siarry, A survey on optimization metaheuristics, *Inf. Sci.* 237 (2013) 82–117.
- [2] S. Mahdavi, M.E. Shiri, S. Rahnamayan, Metaheuristics in large-scale global continuous optimization: A survey, *Inf. Sci.* 295 (2015) 407–428.
- [3] S. Mirjalili, Moth-flame optimization algorithm: A novel nature-inspired heuristic paradigm, *Knowl.-Based Syst.* 89 (2015) 228–249.
- [4] K.T. Gkaragkounis, E.M. Papoutsis-Kiachagias, K.C. Giannakoglou, The continuous adjoint method for shape optimization in Conjugate Heat Transfer problems with turbulent incompressible flows, *Appl. Therm. Eng.* 140 (2018) 351–362.
- [5] S.-M. Lee, K.-Y. Kim, S.-W. Kim, Multi-objective optimization of a double-faced type printed circuit heat exchanger, *Appl. Therm. Eng.* 60 (2013) 44–50.
- [6] A. Biswas, K.K. Mishra, S. Tiwari, A.K. Mishra, Physics-inspired optimization algorithms: a survey, *J. Optim.* (2013) 16.
- [7] I. Fister Jr., X.-S. Yang, I. Fister, J. Brest, D. Fister, A brief review of nature-inspired algorithms for optimization, *Elektrotehniski Vestnik* 80 (3) (2013) 1–7.
- [8] S. Salcedo-Sanz, Modern meta-heuristics based on nonlinear physics processes: a review of models and design procedures, *Phys. Rep.* 655 (2016) 1–70.
- [9] F. Glover, Future paths for integer programming and links to artificial intelligence, *Comput. Oper. Res.* 13 (1986) 533–549.
- [10] R. Storn, K.V. Price, Differential evolution – A simple and efficient heuristic for global optimization over continuous spaces, *J. Global Optim.* 11 (1997) 341–359.
- [11] J.H. Holland, Genetic algorithms, *Sci. Am.* 267 (1992) 66–72.
- [12] R.C. Eberhart, J. Kennedy, A new optimizer using particle swarm theory, in: Proceedings of the Sixth International Symposium on Micro Machine and Human Science (1995), Nagoya, Japan, 39–43.
- [13] M. Asadi, Y. Song, B. Sundén, G. Xie, Economic optimization design of shell-and-tube heat exchangers by cuckoo-search-algorithm, *Appl. Therm. Eng.* 73 (2014) 1032–1040.
- [14] R.V. Rao, V.K. Patel, Thermodynamic optimization of cross-flow plate-fin heat exchanger using particle swarm optimization, *Int. J. Heat Transf.* 49 (2010) 1712–1721.
- [15] G.N. Xie, B. Sundén, Q.W. Wang, Optimization of compact heat exchangers by a genetic algorithm, *Appl. Therm. Eng.* 28 (2008) 895–906.
- [16] M. Mishra, P.K. Das, S. Sarangi, Second law based optimisation of crossflow plate-

- fin heat exchanger design using genetic algorithms, *Appl. Therm. Eng.* 29 (2009) 2983–2989.
- [17] P. Wildi-Tremblay, L. Gosselin, Minimizing shell-and-tube heat exchanger cost with genetic algorithms and considering maintenance, *Int. J. Energy Res.* 41 (2007) 867–885.
- [18] B. Allen, L. Gosselin, Optimal geometry and flow arrangement for minimizing the cost of shell-and-tube condensers, *Int. J. Energy Res.* 32 (10) (2008) 958–969.
- [19] P.D. Chauduri, U. Diwekar, J. Logsdon, An automated approach for the optimal design of heat exchangers, *Ind. Eng. Chem. Res.* 36 (1997) 3685–3693.
- [20] R. Selbas, O. Kizilkiran, M. Reppich, A new design approach for shell-and-tube heat exchangers using genetic algorithms from economic point of view, *Chem. Eng. Process.* 45 (2006) 268–275.
- [21] A.C. Caputo, P.M. Pelagagge, P. Salini, Heat exchanger design based on economic optimization, *Appl. Therm. Eng.* 27 (2007) 1151–1159.
- [22] M. Fesanghary, E. Damangir, I. Soleimani, Design optimization of shell and tube heat exchangers using global sensitivity analysis and harmony search algorithm, *Appl. Therm. Eng.* 29 (5–6) (2009) 1026–1031.
- [23] V.K. Patel, R.V. Rao, Design optimization of shell-and-tube heat exchanger using particle swarm optimization technique, *Appl. Therm. Eng.* 30 (2010) 1417–1425.
- [24] A.S. Sahin, B. Kilic, U. Kilic, Design and economic optimization of shell and tube heat exchangers using Artificial Bee Colony (ABC) algorithm, *Energy Convers. Manage.* 52 (2011) 3356–3362.
- [25] A. Hadidi, A. Nazari, Design and economic optimization of shell-and-tube heat exchangers using biogeography-based (BBO) algorithm, *Appl. Therm. Eng.* 51 (2013) 1263–1272.
- [26] A. Hadidi, M. Hadidi, A. Nazari, A new design approach for shell-and-tube heat exchangers using imperialist competitive algorithm (ICA) from economic point of view, *Energy Convers. Manage.* 67 (2013) 66–74.
- [27] M. Amini, M. Bazargan, Two objective optimization in shell-and-tube heat exchangers using genetic algorithm, *Appl. Therm. Eng.* 69 (2014) 278–285.
- [28] D.K. Mohanty, Application of firefly algorithm for design optimization of a shell and tube heat exchanger from economic point of view, *Int. J. Therm. Sci.* 102 (2016) 228–238.
- [29] D.K. Mohanty, Gravitational search algorithm for economic optimization design of a shell and tube heat exchanger, *Appl. Therm. Eng.* 107 (2016) 184–193.
- [30] E.H. Vasconcelos Segundo, A.L. Amoroso, V.C. Mariani, L.S. Coelho, Economic optimization design for shell-and-tube heat exchangers by a Tsallis differential evolution, *Appl. Therm. Eng.* 111 (2017) 143–151.
- [31] J.J.C. Barros, M.L. Coira, M.P.C. López, A.C. Gochi, Sustainability optimisation of shell and tube heat exchanger, using a new integrated methodology, *J. Cleaner Prod.* 200 (2018) 552–567.
- [32] M.O. Petirin, T. Bello-Ochende, A.A. Dare, M.O. Oyewola, Entropy generation minimization of shell-and-tube heat exchanger in crude oil preheat train using firefly algorithm, *Appl. Therm. Eng.* 145 (2018) 264–276.
- [33] R.V. Rao, V.K. Patel, Thermodynamic optimization of plate-fin heat exchanger using teaching-learning-based optimization (TLBO) algorithm, *Int. J. Adv. Therm. Sci. Eng.* 2 (2011) 91–96.
- [34] M. Yousefi, A.N. Darus, H. Mohammadi, Second law based optimization of plate fin heat exchanger using Imperialist Competitive Algorithm, *Int. J. Phys. Sci.* 6 (20) (2011) 4749–4759.
- [35] M. Yousefi, R. Enayatifar, A.N. Darus, Optimal design of plate-fin heat exchangers by a hybrid evolutionary algorithm, *Int. Commun. Heat Mass Transf.* 39 (2012) 258–263.
- [36] M. Yousefi, R. Enayatifar, A.N. Darus, A.H. Abdullah, Optimization of plate-fin heat exchangers by an improved harmony search algorithm, *Appl. Therm. Eng.* 50 (2013) 877–885.
- [37] H. Zarea, F.M. Kashkooli, A.M. Mehryar, M.R. Saffarian, E.N. Beherghani, Optimal design of plate-fin heat exchangers by a Bees Algorithm, *Appl. Therm. Eng.* 69 (2014) 267–277.
- [38] S. Banoooni, H. Zarea, M. Molana, Thermodynamic and economic optimization of plate fin heat exchangers using the Bees algorithm, *Heat Transf. – Asian Res.* 43 (5) (2014) 427–446.
- [39] E.H. Vasconcelos Segundo, A.L. Amoroso, V.C. Mariani, L.S. Coelho, Thermodynamic optimization design for plate-fin heat exchangers by Tsallis JADE, *Int. J. Therm. Sci.* 113 (2017) 136–144.
- [40] H. Peng, X. Ling, E. Wu, An improved particle swarm algorithm for optimal design of plate-fin heat exchangers, *Indus. Eng. Chem. Res.* 49 (2010) 6144–6149.
- [41] L. Zhang, C. Yang, J. Zhou, A distributed parameter model and its application in optimizing the plate-fin heat exchanger based in the minimum entropy generation, *Int. J. Therm. Sci.* 49 (2010) 1427–1436.
- [42] S. Ghosh, I. Ghosh, D.K. Pratihar, B. Maiti, P.K. Das, Optimum stacking pattern for multi-stream plate-fin heat exchanger through a genetic algorithm, *Int. J. Therm. Sci.* 50 (2011) 214–224.
- [43] V.A. Tucker, Gliding flight: speed and acceleration of ideal falcons during diving and pull out, *J. Exp. Biol.* 201 (1998) 403–414.
- [44] V.A. Tucker, Gliding flight: drag and torque of a hawk and a falcon with straight and turned heads, and a lower value for the parasite drag coefficient, *J. Exp. Biol.* 203 (2000) 3733–3744.
- [45] V.A. Tucker, The deep fovea, sideways vision and spiral flight paths in raptors, *J. Exp. Biol.* 203 (2000) 3745–3754.
- [46] V.A. Tucker, A.E. Tucker, K. Akers, J.H. Enderson, Curved flight paths and sideways vision in peregrine falcons (*Falco Peregrinus*), *J. Exp. Biol.* 203 (2000) 3755–3763.
- [47] C.M. White, N.J. Clum, T.J. Cade, W.G. Hunt, Peregrine Falcon (*Falco peregrinus*), in: A. Poole, E. Gill (Eds.), *The Birds of North America*, No. 660, The Birds of North America Inc. Philadelphia, PA USA (2002).
- [48] D.H. Wolpert, W.G. Macready, No free lunch theorems for optimization, *IEEE Trans. Evol. Comput.* 1 (1) (1997).
- [49] R.K. Sinnott, J.M. Coulson, J.F. Richardson, *Chemical Engineering Design* vol. 6, Butterworth-Heinemann, Boston, USA, 1996.
- [50] F.P. Incropera, D.P. DeWitt, *Fundamentals of Heat and Mass Transfer*, John Wiley and Sons Inc., Hoboken, USA, 2010.
- [51] R. Manglik, A. Bergles, Heat transfer and pressure drop correlations for the rectangular offset strip fin compact heat exchanger, *Exp. Therm. Fluid Sci.* 10 (2) (1995) 171–180.
- [52] A. Bejan, *Entropy generation units: the method of thermodynamic optimization of finite-size systems and finite-time process*, CRC Press, 1995.
- [53] X.S. Yang, A new metaheuristic bat-inspired algorithm, in: J.R. Gonzalez (Ed.), *Nature-inspired cooperative strategies for optimization (NICSO 2010)*, Springer, SCI, 2010, pp. 28465–28474.
- [54] X.S. Yang, Firefly algorithm, stochastic test functions and design optimization, *Int. J. Bio-Inspired Comput.* 2 (2010) 78–84.
- [55] D.Q. Kern, *Process heat transfer*, McGraw-Hill, 1950.
- [56] R.K. Shah, D.P. Sekulic, *Fundamentals of Heat Exchanger Design*, John Wiley & Sons Inc., Hoboken, USA, 2003.
- [57] S. Kakac, H. Liu, *Heat exchanger selection rating and thermal design*, CRC Press LLC, Florida, 2002.